Thesis/
Reports
Catchpole,
E.A.

FINAL REPORT FOR RESEARCH AGREEMENT
#INT-91558-RJVA
"Fire Model Analysis"
UNIVERSITY OF NEW SOUTH WALES
FS Contact: Mr. Richard C. Rothermel
CoOp Contact: DR. E. A. Catchpole

The second generation U.S. firespread model

Final report 1994

INT-91558-RJVA

E.A. Catchpole and W.R. Catchpole

Department of Mathematics and Statistics
University College
The University of New South Wales

April 4, 1995

Chapter 1

The physical model

1.1 Volume element

At this stage we are concentrating on developing a model for the the steady spread of fire through a homogeneous fuel bed, although there has been some preliminary work on heterogeneous fuels (see Catchpole & Catchpole 1991, and Catchpole *et al* 1993).

The fuel bed is modelled as an arrangement of homogeneous particles all with the same moisture content m at ambient temperature. The role of the air between the fuel particles is to supply oxygen; the thermal capacity of this air is neglected. The packing of the fuel is allowed for by defining the bulk density (β) of the fuel as the mass of fuel in a unit volume of fuel-bed space containing both fuel particles and air. Because the surface area of fuel available for burning is an important characteristic, the average value of the particles' surface area to volume ratio (s) is also relevant.

The analysis usually concentrates on a small volume element containing fuel particles and air, as shown in Figure 1.1. Some models position this volume element next to the upper surface of the fuel bed (a), some place it within the fuel bed (b), and others assume it to have small dimensions in the horizontal directions but extend from the top to the bottom of the fuel (c). For the most part we consider only a surface volume element (a). To each element is associated a temperature depending on its position and the time since initial ignition of the fuel bed.

The model is based on the following description of flame propagation. Combustion releases heat energy from the region of burning fuel. Some of this heat is absorbed by the unburnt fuel causing its temperature to rise. When the fuel temperature of a volume element reaches a critical value T_{ig} (the ignition temperature) the particles in the element emit ignitable gases.

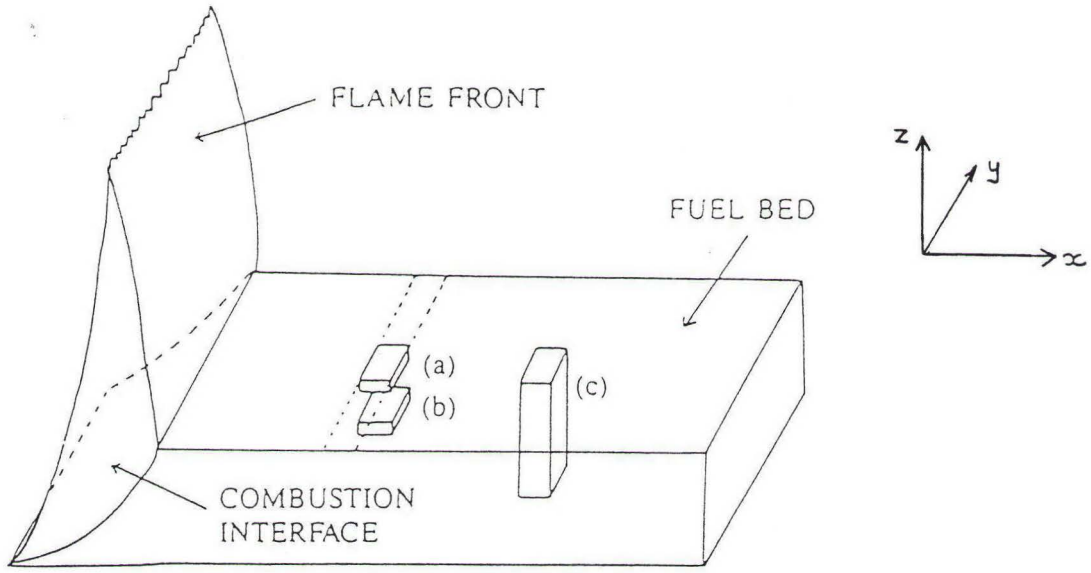


Figure 1.1: (a) Volume element on the surface, (b) volume element within the fuel bed, and (c) total-depth element.

These are ignited by pilot ignition and the particle moves into the combustion zone, and is consumed by an exothermic combustion process. The line on the upper surface of the fuel bed separating burning fuel from unburnt fuel gives the position of the fire front. This fire front propagates at a steady speed. Our main aim is to predict this rate of spread.

1.2 Ignition temperature

Let us now look a little more closely at the heating of such fuel particles up to ignition temperature. Each particle is assumed to be at uniform temperature throughout its volume. For non-fine fuels this assumption is unrealistic, and modifications will be discussed later.

Far away from the fire the particles are at ambient temperature but, as the flame front approaches, the particles increase in temperature until the boiling point of water is reached. At this stage we might adopt the simple assumption that further input of heat energy firstly drives off all the water at this temperature and then raises the dry fuel element to ignition temperature. The heat required to raise the fuel-element temperature in the models is illustrated schematically in Figure 1.2. Thus the relationship between heat and temperature is step-wise linear.

More precisely, if a net amount of heat dQ per unit mass of fuel bed is transferred from the combustion zone or flame to the fuel bed element, then the corresponding rise in temperature dT is given by (see e.g. de Mestre *et*

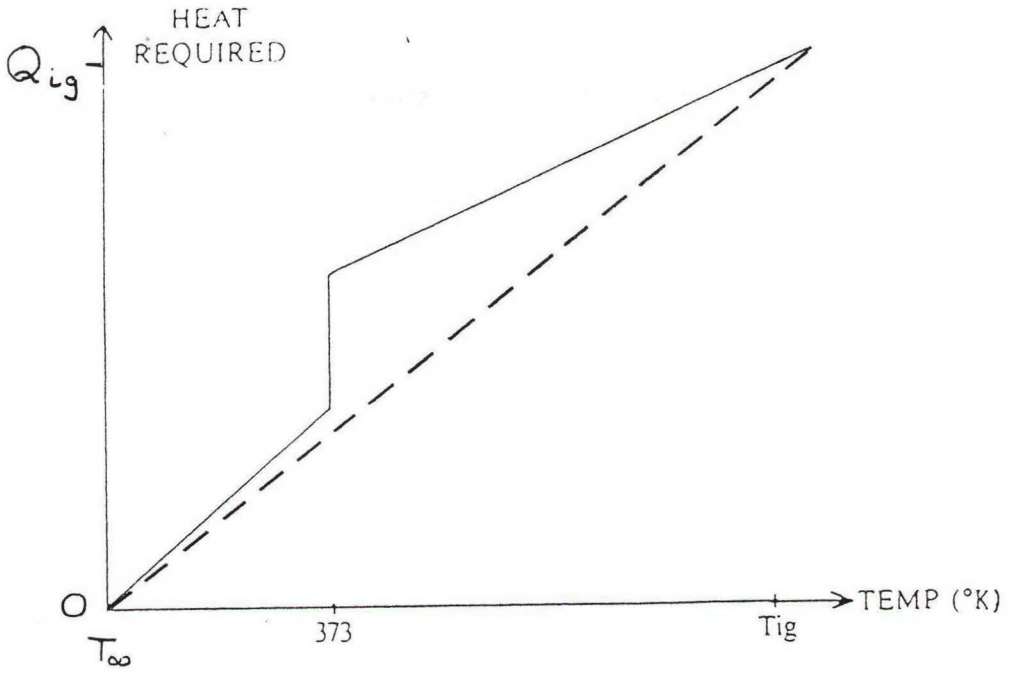


Figure 1.2: Heat required to raise unit mass of fuel from ambient to ignition temperature, versus fuel temperature attained. The vertical step is due to the latent heat of water.

al, 1989)

$$dQ = \begin{cases} (c_p + mc_w)dT, & T_\infty < T < 373 \\ -\mathcal{L}dm, & T = 373 \\ c_p dT, & 373 < T < T_{\text{ig}} \end{cases} \tag{1.1}$$

where

c_p = specific heat of dry fuel

c_w = specific heat of water

$\mathcal{L}$ = latent heat of water

m = moisture content of fuel
(= mass of water per unit mass of fuel)

A simpler model for the rise of temperature with heat input is just to assume a linear relationship:

$$dQ = c^* dT, \quad T_\infty < T < T_{\text{ig}}, \tag{1.2}$$

as shown by the dashed line in Figure 1.2. Here c^* denotes an "average specific heat", which accounts also for the latent heat of water. Its value is found by integrating (1.1) and (1.2) from ambient temperature T_∞ to ignition temperature $T_{\rm ig}$:

$$Q_{\rm ig} = (c_p + mc_w)(373 - T_\infty) + \mathcal{L}m + c_p(T_{\rm ig} - 373). \tag{1.3}$$

$$Q_{\rm ig} = c^*(T_{\rm ig} - T_\infty) \tag{1.4}$$

Here $Q_{\rm ig}$ is the quantity of heat required to raise unit mass of fuel[1] to ignition temperature, sometimes called the "heat of ignition" of the fuel. Equation (1.3) was given by Dunlap (1912). Experiments indicate that for typical fuels equation (1.2) is a better approximation of particle temperature rise than (1.1) — see de Mestre *et al* (1989).

A crucial but frequently unstated assumption in almost all physical models of fire spread is that there is a well-defined ignition temperature, at which a particle bursts into flame regardless of preceding conditions. In particular, ignition takes place at this temperature regardless of how quickly or slowly the particle has been heated. Since water vapour is the first pyrolizate, a particle heated slowly will have lost almost all moisture before ignitable gases are given off; a rapidly heated particle on the other hand will still be losing water vapour from its deeper layers while the surface is giving off ignitable gas. These gases will therefore be diluted with water vapour, and may require a higher temperature to ignite them.

It is thus highly plausible that ignition temperature increases as the rate of spread increases. The magnitude of this effect in unknown; to our knowledge no experiments have explored this. The most relevant results are those of Frandsen (1973).

1.3 Heat transfer mechanisms

(i) Radiative heating

A difficult problem in the physical modelling of fire propagation is in determining the physical processes governing heat transfer. For the transfer of heat from the flame to the fuel element all models include radiative heating. Some models also include convective heating — short-range heating by hot gases emerging from the flame front (flame contact, or turbulent diffusion), and, for wind-driven fires, the longer-range heating caused by hot air from the flaming region being advected over the unburned fuel.

[1]The unit mass does not include the mass of water

As with most previous models, we treat radiation from the flame as emanating from an opaque surface coincident with the average position of the front of the flame. This surface is taken to be a plane of finite length and finite or infinite width, inclined at an angle ϕ_f (say) to the vertical. In a wind blown fire ϕ_f is positive.

The flame surface is taken to radiate as a grey body, with a (nominal) surface temperature T_f and emissivity ϵ_f. These may be taken to be constant over the whole surface, or to depend on height above the fuel surface. The hemispherical rate of radiation from a given point on the flame surface will then be given by

$$E_f = \epsilon_f \sigma_B T_f^4 \tag{1.5}$$

per unit area of flame surface, where σ_B is the Stefan-Boltzmann constant.

A more accurate model might treat the flame radiation as gas phase radiation. The standard model for a uniform gas gives

$$\epsilon_f = 1 - e^{-kD}, \tag{1.6}$$

where D is the width of the flame in the direction of a particular beam, as shown in Figure 1.3.

Note that this approaches zero for a very small D and approaches 1 (the value for a perfect black body radiator) for very thick flames. Thus ϵ_f varies not only with distance above the fuel bed but also with the direction of the beam of radiation. Such a model would be very difficult to implement. As a compromise, we could model the radiation from the flame as coming from a solid sheet, but acknowledge the diffuse nature of the flame by assuming that the flame sheet has an emissivity ϵ_f given by (1.6), where $D = D_f$, the flame depth in a horizontal direction at the base of the flame (see Figure 1.3).

We model the radiation from the combustion zone in a similar way to that from the flame, by assuming that the combustion interface is a plane, inclined at an angle ϕ_b to the vertical, and that the radiation can be approximated by that from a solid sheet on this plane, at temperature T_b and of emissivity ϵ_b. Although combustion interfaces are known to be curved in general (see for example Albini 1985, 1986), the error caused by our assumption will be small in most cases, since we are considering only the heat received by a surface fuel element (see Figure 1.4).

There are two commonly used approaches to modelling the absorption of radiation from the flame by the fuel, which we term "surface heating" and "volume heating". In the surface-heating mechanism the radiation is transmitted (undiminished) from the flame front to the surface of the unburnt fuel bed. The fuel surface heats up and acts as a source which then heats the remainder of the fuel bed.

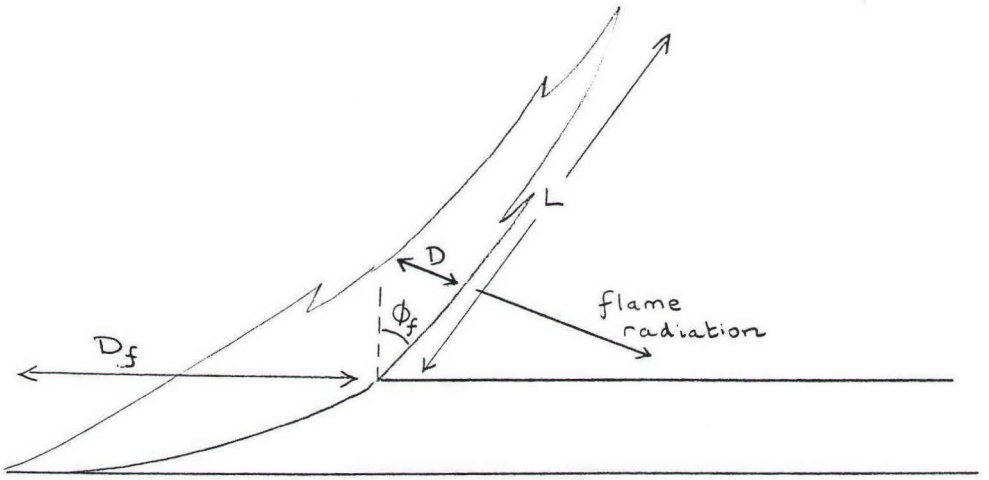


Figure 1.3: Radiation from a diffuse flame, showing two possible measures of flame depth.

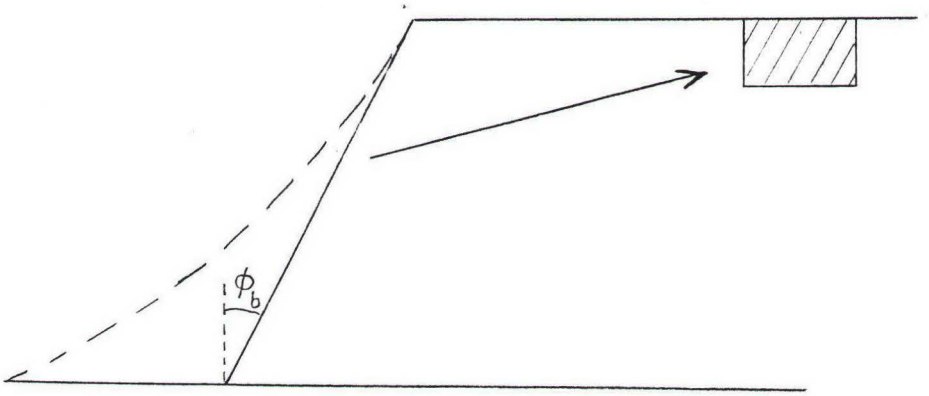


Figure 1.4: Radiation from the combustion interface to a surface fuel element.

The volume-heating mechanism is more realistic but mathematically more difficult. It postulates a semi-transparent fuel bed through which the rays penetrate until they meet a fuel particle, which absorbs the radiation and rises in temperature. Thus the radiation gradually diminishes as it passes through the fuel bed. This model is greatly simplified if the fuel particles are assumed to act as black-body absorbers, so that there is no reflection or scattering of radiation.

The mathematical law appropriate for the absorption of a beam of radiation through such a semi-transparent medium is that of exponential decay,

$$i = i_0 e^{-\alpha r} \tag{1.7}$$

where i is the intensity of a beam of radiation, r is the distance that the beam has travelled through the fuel bed, and α is a decay constant (α^{-1} is the mean free path length for radiation through the fuel). For a collection of randomly oriented, black, convex particles, it can be shown (see e.g. Hottel *et al* 1965) that $\alpha = s\beta/4$, where s is the surface-area to volume ratio of the particles and β is the packing ratio, so that $s\beta$ is the surface area of fuel per unit volume of fuel bed.

(ii) Convective heating

The rate of convective heat input per unit volume of fuel bed is

$$q_c = \hbar s\beta(T_a - T), \tag{1.8}$$

where $\hbar$ is the convective heat transfer coefficient, T is the temperature of the particles in the unit volume, and T_a is the temperature of the surrounding gas. This gas may range from a mixture of air and pyrolised gases at flame temperature, moving at fairly high velocity and turbulent, to still air at ambient temperature (in which case q_c becomes a cooling term).

The convective heat transfer coefficient $\hbar$ depends mainly on particle size and on the gas velocity. It can be calculated from empirical formulæ relating the Nusselt and Reynolds numbers. The Nusselt number

$$N_u = \frac{\hbar \ell}{k} \tag{1.9}$$

is a dimensionless measure of the gas temperature gradient at the fuel surface. Here k is the thermal conductivity of the gas, and ℓ is a characteristic fuel particle dimension. The Reynolds number

$$R_e = \frac{U_0 \ell}{\nu} \tag{1.10}$$

is the ratio of inertial to viscous force. Here U_0 is the gas flow speed past the particles and ν is the kinematic viscosity of the gas.

For example, for a cylindrical particle in a crossflow, using $\ell = d$, the particle diameter, Incropera and de Witt (1990, equation 7.56) give an empirical relation which reduces, for air at atmospheric pressure in the range 300–1000 K, to

$$N_u \approx 0.66 R_e^{0.4}, \tag{1.11}$$

valid for $1 < R_e < 40$. This gives

$$\hbar \approx 0.66 k \nu^{-0.4} d^{-0.6} U_0^{0.4} \approx 0.29 k \nu^{-0.4} s^{0.6} U_0^{0.4}, \tag{1.12}$$

where we have used $s \approx 4/d$ for a long thin cylinder. For a particle of diameter 1 mm, typical of pine needles, the range $1 < R_e < 40$ corresponds to a gas velocity of roughly 0.05–2 m/sec, depending on the gas temperature. More complicated empirical relations are available which cover the entire range of Reynolds numbers for which data are available (see e.g. Incropera and de Witt, 1990, equation 7.57).

To calculate $\hbar$ from (1.12), we need to know U_0, the local gas velocity. One possibility is to use the free stream velocity U, scaled to a value at the fuel surface by means of the standard logarithmic profile for flow over a vegetation canopy (see e.g. Monteith and Unsworth, 1990). Another possibility is to use the equations of fluid dynamics to model the flow within the canopy (see e.g. Raupach and Shaw, 1982).

Having calculated a value for $\hbar$, it remains, in order to quantify the convective heating, to measure or predict the local gas temperature T_a in the vicinity of the fuel particles. (In our laboratory experiments, we have measured both T_a and U_0, but a predictive model must predict them.) Diffusive heating, from turbulent flames, can be modelled by letting $T_a = T_f$, flame temperature, together with a Gaussian decay with distance from the flame, representing a decreasing probability of flame contact. Advective heating can be modelled in a similar simple way, with a slower (usually exponential) decay.

(iii) Heat losses

Loss due to re-radiation from the element varies as the difference $T^4 - T_\infty^4$ between the fourth powers of the absolute temperature of the element and that of the environment. Heat loss due to convective cooling by the surrounding air (assumed to be at ambient temperature) is proportional to the difference $T - T_\infty$. A calculation by Albini (1986) showed that the natural convective cooling of foliage is of comparable magnitude to the radiative cooling, throughout the range from ambient to ignition temperature.

The relative simplicity of linear differential equations encourages us to approximate radiative cooling in a linear fashion, using

$$T^4 - T_\infty^4 \approx T_i^4 - T_\infty^4 + 4T_i^3(T - T_i), \tag{1.13}$$

where T_i is any intermediate value between ambient and ignition temperatures — e.g. 373 K.

1.4 Energy balance equations

The model is based on the energy balance of a typical fuel volume element. The net effect of heat input and heat loss in a small interval of time is equated to the corresponding increase in internal energy of the fuel element as given by (1).

This energy balance leads to a differential equation for the average temperature of the volume element, which contains the rate of spread as a parameter. When the rate of spread is assumed constant, the differential equation can be integrated as the flame front moves from the far distance, when the temperature of the volume element is ambient, towards the volume element. When the flame reaches the volume element, the temperature reaches ignition temperature and the volume element bursts into flame. This is often referred to as an integrated or global energy balance. The only unknown in the resulting equation is the (constant) rate of spread, and so this equation serves to determine the rate of spread. The rate of spread may then be substituted back into the differential equation, whose solution will then give an explicit prediction of the fuel temperature field ahead of the flame front.

A simple approach to the derivation of the differential equation is as follows. Consider a volume element at location (x, y, z) in the fuel bed, where the coordinate system is as shown in Figure 1.1 — thus x is measured in the same direction as the fire propagation, y is horizontal, parallel to the flame front, and z is vertical. Let the temperature, at time t, of the fuel particles in the volume element be $T(x, y, z, t)$, and the corresponding heat content be $Q(x, y, z, t)$ per unit mass of fuel, where Q and T are related by (1.1). The heat content *per unit volume* of fuel bed is then $\rho_b Q$, where ρ_b is the bulk density of the fuel bed, that is the mass of fuel per unit volume of fuel bed. In the 2-dimensional situation, where the fire front is straight and infinitely wide, the temperature cannot depend on the lateral position of the fuel particle and so we have $T(x, z, t)$ only. The rate of temperature rise $\partial T/\partial t$ of the fuel element is then related to the net rate of heat absorption

per unit volume of fuel bed, $\partial Q/\partial t$, by

$$\frac{\partial Q}{\partial t} = c^* \frac{\partial T}{\partial t}, \tag{1.14}$$

as in (1.2).

We consider only the quasi-steady case, when the fire has reached a steady rate of spread R. In this case the distance X of the volume element from the flame front is decreasing linearly with time

$$X = X_0 - Rt,$$

and it follows that

$$\frac{\partial T}{\partial t} = -R\frac{\partial T}{\partial X}.$$

The coordinates (X, z) define a moving coordinate system, in which the flame front is fixed and the fuel element approaches the flame front at speed R. In this new coordinate system the rate of heat absorption is given by

$$\frac{\partial Q}{\partial t} = -R\frac{\partial Q}{\partial X} = -Rc^*\frac{\partial T}{\partial X}. \tag{1.15}$$

The modelling effort then focusses on modelling the heat transfer processes from the flame and combustion zone to the fuel element (and heat losses from the fuel element), in order to find $\dfrac{\partial Q}{\partial t}$. Once this is done, the governing differential equation takes the form

$$-R\rho_b c^* \frac{\partial T}{\partial X} = q(X, z), \tag{1.16}$$

where $q(X, z)$ is the net rate of heat input per unit volume of fuel bed at the point (X, z). This net heat inflow is broken down according the the heat transfer mechanism,

$$q = q_r + q_c - q_\ell, \tag{1.17}$$

where $q_r = q_f + q_b$ is the total radiant heat input (energy per unit time per unit volume) into the volume element, q_f and q_b being the contributions from the flame and combustion zone, respectively; q_c is the convective heat transfer, and q_ℓ is the radiative heat loss from the fuel element. Note that q_c may be positive (in a wind-driven fire) from hot air which has passed through the combustion to the fuel (advective heating) or due to short range (diffusive) heating caused by turbulence in the flame, or it may be negative to account for heat loss from the warm fuel to the surrounding cooler air; or

it may account for all of these, for example switching from negative (cooling) far away from the flame to positive (heating) close to the flame.

Integrating (1.16) over the whole of the unignited portion of the fuel bed gives

$$Rw Q_{\text{ig}} = \iint q(X, z)\, dX dz, \tag{1.18}$$

where $w = \rho_b h$ is the total fuel loading per unit area of the fuel bed, h being the depth of the fuel bed.

For non-fine fuels the left-hand side of (1.18) overestimates the amount of heat absorbed by the fuel during the preheating process. Many authors replace w in (1.18) by w_a, the actual amount of fuel consumed in the fire. This is certainly an improvement, but is still an overestimate. Better is to replace w by ηw, where η is the effective proportion of the fuel raised to ignition temperature during the preheating process. Frandsen (1973) gives empirical values for η for several fuels used in laboratory fires. Thomas (1967) uses a physical argument to estimate η.

Equation (1.18) is the integrated energy balance equation. It states simply that the rate at which fuel is being heated to ignition temperature, and consumed in the combustion zone, is equal to the total net rate of heat transfer from the combustion zone and flames into the unignited portion of the fuel bed. In the simplest models this equation is used to determine the rate of spread R. In less simple models however, the rate of energy transfer q depends on the fuel temperature T, for example through the convective heating term (1.8). Then (1.18) is inappropriate; instead the differential equation (1.16) must be solved directly.

For a surface fuel element, putting $z = 0$ in (1.16) and integrating from $X = 0$ to ∞ gives

$$R\rho_b \eta Q_{\text{ig}} = \int_0^\infty q(X)\, dX, \tag{1.19}$$

where $q(X) = q(X, 0)$, and again we have used the factor η to account for the preheating of only a fraction of non-fine fuels.

The left-hand side of (1.19) is called the *propagating flux* I_P, and can be thought of as the rate of transfer of sensible heat through a unit surface area perpendicular to the direction of flame travel.

1.5 A simplified model

We consider a surface fuel element, and replace (1.16) by

$$-R\rho_b \eta c^* \frac{dT}{dX} = q(X), \tag{1.20}$$

which implies that only a fraction η of each fuel particle is involved in the preheating process. At this stage we neglect radiative heating from the combustion zone, and neglect any radiative losses. Then (1.20) becomes

$$-R\rho_b\eta c^* \frac{dT}{dX} = q_f(X, L, \phi_f) + 4\alpha\hbar(X)(T_a(X) - T(X)), \tag{1.21}$$

where we have used (1.8) for the convective heating term, and have explicitly referred to the dependence of the radiative heating term q_f on the flame length L and flame angle ϕ_f, as well as on the distance from the fire front X.

This equation can be integrated directly to give

$$R\rho_b\eta Q_{\rm ig} = \int_0^\infty q_f(X, L, \phi_f)\, dX + 4\alpha \int_0^\infty \hbar(X)(T_a(X) - T(X))\, dX \tag{1.22}$$

Note that this equation contains the unknown temperature field $T(X)$ on the right-hand side, and so cannot be used to find the rate of spread R, unless this temperature field can be predicted in some empirical way. To derive an integrated energy balance equation which does not contain $T(X)$ on the right-hand side we proceed as follows. It is convenient to reset the origin by letting $\Theta = T - T_\infty$ be the temperature of the fuel element in excess of ambient temperature. Equation (1.21) can be written

$$-R\rho_b\eta c^* \frac{d\Theta}{dX} = q_f + 4\alpha\hbar(X)(\Theta_a(X) - \Theta(X)),$$

or

$$-\frac{d\Theta}{dX} = kq_f + 4\alpha k\hbar(X)(\Theta_a(X) - \Theta(X)), \tag{1.23}$$

where $k = 1/(R\rho_b\eta c^*)$. Now let

$$\bar{H}(X) = \int_0^X \hbar(u)\, du.$$

Then multiplying (1.23) throughout by $\exp(-4\alpha k\bar{H}(X))$ gives

$$e^{-4\alpha k\bar{H}} \left(\frac{d\Theta}{dX} - 4\alpha k\hbar\Theta \right) = -e^{-4\alpha k\bar{H}}(kq_f + 4\alpha k\hbar\Theta_a), \tag{1.24}$$

where we have omitted dependencies on X. Now the left hand side is the exact differential of $e^{-4\alpha k\bar{H}(X)}\Theta(X)$, and so integrating from $X = 0$ to ∞ gives

$$\left[e^{-4\alpha k\bar{H}(X)}\Theta(X)\right]_{X=0}^{\infty} = -k\int_0^\infty e^{-4\alpha k\bar{H}(X)}\left(q_f(X) + 4\alpha\hbar(X)\Theta_a(X)\right) dX \tag{1.25}$$

Note that $\bar{H}(X) > 0$ for all X and that $\Theta(X) \to 0$ as $X \to \infty$, and also that $\bar{H}(0) = 0$. Thus the left side of (1.25) reduces to $-\Theta(0) = -(T_{\rm ig} - T_\infty)$. Consequently, on dividing through by k, (1.25) gives

$$R\rho_b\eta Q_{\rm ig} = \int_0^\infty e^{-4\alpha k\bar{H}(X)} q_f(X)\, dX + 4\alpha \int_0^\infty e^{-4\alpha k\bar{H}(X)} \hbar(X)(T_a(X) - T_\infty(X))\, dX. \tag{1.26}$$

Note that if $\hbar$ does not depend on X then the directly integrated energy balance equation (1.22) becomes

$$R\rho_b\eta Q_{\rm ig} = \int_0^\infty q_f(X, L, \phi_f)\, dX + 4\alpha\hbar \int_0^\infty (T_a(X) - T(X))\, dX \tag{1.27}$$

while in the energy balance equation derived via the integrating factor, we have $\bar{H}(X) = \hbar X$ and so (1.26) becomes

$$R\rho_b\eta Q_{\rm ig} = \int_0^\infty e^{-\lambda X} q_f(X)\, dX + 4\alpha\hbar \int_0^\infty e^{-\lambda X}(T_a(X) - T_\infty(X))\, dX, \tag{1.28}$$

where $\lambda = 4\alpha k\hbar = 4\alpha\hbar/(R\rho_b\eta c^*)$.

Equations (1.26) and (1.28) contain only the unknown rate of spread R, and not the temperature field $T(X)$, and so can be solved for R. Note however that R is involved in both integrals in (1.26) and (1.28), through k in (1.26) and through λ in (1.28). Thus it will be necessary to solve these equations via some numerical scheme.

1.6 Modelling the radiative heating from the flame

We considered four possible models for the absorption of radiation from the flame by the surface fuel element.

slab bed

In this model the fuel surface is assumed to be a solid surface, which absorbs radiation from the flame. The heat is transmitted down through the fuel by some unspecified mechanism to heat the rest of the bed. This model was used by Hottel *et al* (1965), Van Wager (1967) and Thomas (1967), amongst others. Regardless of the merits of this model (and we would argue that it is unrealistic for most naturally-occurring fuels, and also for our laboratory fuel beds), this is a whole-bed model, not a surface heating model.

modified slab bed

Here the radiation is assumed to be absorbed as though the fuel surface were solid, but the amount absorbed is multiplied by the factor α to allow for the porosity of the fuel bed. This model was used by Rothermel (1971). It is similar (but not equivalent) to the slab model with heat transfer assumed to be vertical radiation through the bed. It is equivalent to the volume heating model if the radiation impinges vertically onto the fuel bed surface.

volume heating

The radiation passes through the fuel bed, being absorbed at a rate of α per unit length, and so heating the fuel. (Reflection is ignored — thus the fuel particles are assumed to behave approximately as black bodies.) This model was used by Albini (1985, 1986). Albini included an extra heat transfer term, reradiation from warmed fuel particles, which we have ignored.

surface particle

Instead of a surface volume element, we can instead consider an energy balance for a single fuel particle on the fuel surface. The particle can be regarded as being randomly oriented, in which case the rate of spread would be calculated after taking the expectation over all directions, or, for special purposes, a particular orientation can be considered (see Appendix B).

The rate of radiation being absorbed by an elemental area of the slab surface at X, per unit area of the surface, is given by $E_f J_f(X)$, where E_f is given by (1.5) and $J_f(X)$ is the view factor for two inclined rectangles. If the flame temperature and/or emissivity varies with height above the fuel bed, then the rate of radiation absorption can still be written in the same way, although $J_f(X)$ is no longer a view factor. The values of $J_f(X)$ for both cases are given in Appendix C. For the modified slab bed, the rate of radiation absorption is just $\alpha E_f J_f(X)$, with the same J_f as for the slab bed.

The rate of radiation aborption for the volume heating and single particle models can also be written in the form $\alpha E_f J_f(X)$ in the case of a constant flame temperature and emissivity, and in a similar way for variable flames. Appropriate formulæ for J_f are given in Appendix C for all cases.

1.7 Estimating the terms in the energy balance

Some of the terms in the above models can be estimated directly by instrumentation, others are unknown. Three pairs of thermocouples recording fuel and air temperature from fire initiation to ignition each gave measurements of $T_a(X) - T(X)$ at points X, the positions of the firefront at 1/20th sec intervals. The fuel thermocouples were placed inside pieces of fuel which were mounted flat as rungs of a 'ladder' laid on the fuel bed. The air thermocouples were mounted as close as possible to the fuel thermocouples near the surface of each fuel piece. In fuel beds made of vertical sticks the fuel thermocouples were mounted in the sticks either in the front, back or centre of the sticks, at a depth of approximately 1mm.

The convective heat transfer coefficient $\hbar(X)$ depends on the Nusselt number, N_u at X, and a characteristic length, which we take here to be the particle diameter. In turn the Nusselt number depends on the Reynolds (R_e) and Prandtl (P_r) numbers usually in the form

$$N_u = cR_e^m P_r^m,$$

(see Incropera and DeWitt 1990), or in some more complicated form that incorporates various formulations at different Reynolds numbers. The values of c and m depend on the shape and orientation of the particles. In addition, there may be a correction for enhanced turbulent transfer in packed beds.

Since the Reynolds number depends linearly on the fluid flow around the particles, and this increases as the fire front nears, the convective transfer coefficient $\hbar$ varies with X. However, we can consider an average value of the convective heat transfer coefficient during the time the fuel is heated by convection. Since $T_a - T$ is small far away from the flame, giving a negligible convective heat flux, $\hbar$ may be thought of as an average value of the heat transfer coefficient close to the flame, and thus the approximation may be reasonable.

To determine the principal fluid flow at the fuel bed surface, where the heat transfer is taking place, we used a velocity probe pointing toward the advancing flame (but with an acceptance angle of 60 degrees, so that some of the vertical component of velocity was being measured). We measured average velocity in the period from where $T_a - T > 5K$ to ignition (determined to be when the fuel temperature reached $520K$). In addition we obtained measures of turbulence estimated by the root mean square values of the probes about the smoothed time-dependent mean values.

This enabled us to determine an estimate of $\hbar(X)$ from various formulæ

in Incropera and De Witt, using either the velocity measured by the probes, a modified velocity incorporating the measure of turbulence, or an estimated velocity from the tunnel windspeed corrected for entrainment. In addition the average heat transfer coefficient $\hbar$ could be estimated using average values of the probe velocity.

If constant flame temperature with height is assumed for the radiating flame, either the radiative temperature or the radiation emissive flux E_f needs to be determined. The values $\widehat{E_f}$ of readings from a bolometer measuring radiation at the fire front over a hemisphere were used as estimates of E_f (Butler 1993).

If variable flame temperature with height is assumed, it is necessary to know the flame temperature profile. A simple approximation is to assume that flame temperature falls off linearly with flame height. A study of the temperature profile for 6 fires, using thermocouples at different heights in the flame, showed that this approximation is reasonable (see Figure 1.6). Flame tip temperature was found experimentally to be approximately 550 K, which is close to the temperature of 500 K that Albini (1981) assumed in his flame model. Flame base temperature was estimated from the average thermocouple temperature over the first third of the base of the flame. Further back in the flame the temperature decreased quickly as flaming combustion gave way to smouldering combustion.

1.8 Balancing the energy equations

Before predictive equations can be developed for spread rate it is necessary to estimate the convective heat transfer coefficient $\hbar$. We first used a modified slab bed model, and assumed a constant flame temperature. Several formulae in Incropera and DeWitt were tried for $\hbar$. None of these proved satisfactory and gave 'banana shaped' plots of the measured propagating flux $I_P = R\rho_b\eta Q_{\text{ig}}$ versus the estimated propagating flux from the right-hand side of (1.27) or (1.28).

Because of the position of the bolometer at the base of the flame, the measured radiative emissive flux was thought to be an overestimate of the emissive flux of the whole flame. To counteract this a 'flame length modification factor' b was introduced, so that the radiative flux was modelled as $\alpha E_f J_f(X, bL, \phi_f)$, where bL is the 'effective flame length.' This introduced an unknown parameter into the model equations giving more flexibility.

In addition it was decided that the formulae for $\hbar$ in Incropera and DeWitt may not be appropriate for heat transfer in turbulent incandescent gas, so $\hbar$ was left as an unknown in the model equations (assuming a constant 'average'

$\hbar$ as in (1.27) and (1.28)).

To estimate the two unknowns b and $\hbar$ (1.27) was used to obtain an expression for $\hbar$ in terms of b, and this was substituted in (1.28). The resulting equation was then solved by iteration. Many of the values for b and $\hbar$ obtained from this procedure were poorly determined because of the similar derivation of the two model equations (see Figure 1.7). In some cases no solution could be found. As we had repeat information from 3 thermocouples pairs on each fire, outlying observations could be checked. For thermocouple pairs which had bad values or values for which an equation balance could not be obtained (1.21) (assuming an average $\hbar$) was solved numerically using various values of b and $\hbar$ until a combination was found that gave a good fit by eye to the fuel temperature profile (see Figure 1.8). Thus values for b and $\hbar$ were found for each thermocouple pair for each fire. The flux balance (1.27) obtained from this procedure is shown in Figure 1.9.

It should be noted that any energy balance method of obtaining the terms in the heat fluxes gives estimates that are dependent on the measured flame dimensions. If these flame dimensions are affected by the burning conditions (such as restrictions on buoyancy in the wind tunnel), this will affect the estimates, in which case the parameters in the submodels will not be appropriate for fires in different conditions (for example, in the open).

The average flame length modifier obtained was about 0.5. This procedure was also attempted using the volume heating model for radiative flux, but the values for the flame length modifier were found to be of the order of 0.1 – 0.2, which gave effective flame lengths of 10-20 cm. This seemed unreasonably small, so this formulation wasn't pursued. The single particle model would give similar results, as it gives very similar estimates of radiative flux to the volume heating model.

We also considered a variable temperature model for the flame, using the average measured temperatures at the base of the flame, and a value of 550 K at the top of the flame. (A variable temperature model using a flame temperature submodel is currently under investigation.) This had the advantage that it did not rely on data from the hemispherical bolometers. The hemispherical bolometers gave higher radiative emissivities than we expected from a diffusion flame diluted by entrained air. The correlation with flame length, and the high readings gave rise to the concern that they were being affected by reflected radiation from the ceiling and walls of the tunnel. Overall we had misgivings about the readings from the hemispherical bolometers, and will investigate alternatives in the future.

In the variable flame temperature model we used the volume heating model for radiative heating. The unknowns in the model equations were then $\hbar$ and ϵ_f. These were determined by a least-squares fit of the observed and

fitted temperature profiles in (1.21). Again some of the estimates of $\hbar$ and ϵ_f were poorly determined, and had to be fitted by eye to obtain consistency over all rungs of the ladder. The flux balance using these estimated values is shown in Figure 1.10.

Chapter 2

Submodelling

To obtain a predictive model for the spread rate it is necessary to submodel the terms in either (1.27) or (1.28) to obtain an equation where only the spread rate R is unknown. Submodelling has to be done either in terms of fuel and environmental variables known prior to a fire, or in terms of variables like Byram's intensity I_B that can be written in terms of R. At present the submodelling that has been done is based on the assumptions of a constant flame temperature and modified slab bed heating. Work is proceeding on submodelling assuming a variable flame temperature and volume heating. Submodelling has been based on (1.27).

We shall consider the parameters in (1.27) in turn and discuss the submodels used.

2.1 Byram's intensity

Byram's intensity I_B does not appear in (1.27) but several of the submodels are based on it. It is defined as

$$I_B = h_c w_a R$$

(Brown and Davis 1973), which we can write as

$$I_B = h_c w \eta_\delta R.$$

The fuel heat constent h_c and the dry fuel loading w are known prior to the fire. The spread rate R is to be determined. The efficiency η_δ is principally fuel dependent, and may be estimated as 0.9 for excelsior and 0.7 for sticks and pine needles (see Catchpole *et al*, in preparation).

2.2 Flame length

The view factors (or pseudo-view factors) J_f depend on flame length and flame angle. Flame length models are generally based on Byram's intensity. Two possible candidates are Byram's flame length model (Brown and Davis 1973), which is based on correlations with Byram's intensity, and Albini's model for flame structure from a wind-driven line fire, which in its approximate form, gives flame length in terms of windspeed and Byram's intensity (Albini 1981). Neither of these models fit the laboratory data very well (see Catchpole *et al*, in preparation). Work is proceeding on two fronts: on modifying Albini's approximate model, and on estimating the parameters in the exact form of the model, to produce predictions that are satisfactory for both laboratory and field data.

In the meantime a preliminary model for flame length is given by

$$L = a\,(I_B)^b$$

where a and b are estimated from a regression of flame length on Byram's intensity. For the wind-aided laboratory fires, for which we have a full set of data for model estimation, $\hat{a} = 0.0449$ and $\hat{b} = 0.495$ ($R^2 = 0.84$). The fit of the model to the data is shown in Figure 2.1.

2.3 Flame angle

Albini's (1981) paper gives an approximate model for flame angle ϕ_f in terms of the Froude number based on flame height. Again this model was found to give poor predictions for the laboratory data (see Catchpole *et al*, in preparation), and needs modification. The flame angle is very sensitive to the boundary layer wind profile that is assumed, so the exact model, which includes the velocity profile, may give better results.

Using the results of laboratory experiments in the wind-tunnel in Macon, Georgia, Nelson and Adkins (1986) regressed $\tan\phi_f$ on the Froude number based on flame height. The Froude number, F_r, is equal to $U^2/(gH_f)$, where U is the windspeed, and H_f is the flame height. Nelson and Adkins' regression equation is

$$\tan\phi_f = 0.89(F_r)^{0.29}.$$

A similar regression analysis on our wind-aided fire data produced the weaker relationship

$$\tan\phi_f = 0.88(F_r)^{0.18},$$

with a low $R^2 = 0.46$. The fit of the submodel is shown in Figure 2.2. There is a suggestion there that the submodel may be fuel-dependent.

The submodel for flame angle requires an estimate of flame height which we hoped might be estimated from a modification of Albini's (1981) formula

$$H_f = k\left(\frac{I_B}{U}\right)$$

for some constant k. However, like Nelson and Adkins (1986) we found that this did not produce satisfactory estimates of H_f, and it was necessary to predict H_f from a non-linear equation in $\frac{I_B}{U}$. The resulting prediction equation for H_f was

$$H_f = 0.0358\left(\frac{I_B}{U}\right)^{0.57},$$

with $R^2 = 0.88$ (see Figure 2.3).

2.4 Radiative emissive flux

The hemispherical bolometer readings $\widehat{E_f}$ are estimates of the radiative emissive flux E_f, which, for an idealised solid flame front, is equal to $\sigma_B \epsilon_f T^4$. Surprisingly there was virtually no correlation between $\widehat{E_f}$ and T_f, but this may be because the thermocouples are poor indicators of the radiative flame temperature. A correlation with flame depth might also be expected through a correlation of ϵ_f with flame depth (see, for example Thomas 1963). However the correlation of $\widehat{E_f}$ with flame depth was not strong. In fact $\widehat{E_f}$ was correlated most strongly with flame length (see Figure 2.4), but since flame length itself needs to be submodelled in terms of Byram's intensity, submodelling the $\widehat{E_f}$ in terms of Byram's intensity seemed most appropriate. The regression model used for wind-aided fires was

$$E_f = aI_B^b$$

where $\hat{a} = 1.90$ and $\hat{b} = 0.46$. However there appear to be several outliers, and the correlation is poor, with $R^2 = 0.48$ (see Figure 2.4).

2.5 Flame length modifier b

The flame length modifier depended weakly on packing ratio, surface-area to volume ratio and moisture content. A regression model using the heat sink terms $\rho_b \eta Q_{ig}$ as the dependent variable was tried, but the correlation was poor ($R^2 = 0.19$). A suitable model was difficult to find. For the present purposes the flame length modifier was predicted from the mean flame length modifier for each fuel type. The means were 0.42 for regular excelsior, 0.51 for pine needles and coarse excelsior, and 0.81 for sticks.

2.6 Radiative flux

It can be seen that the radiative flux as determined by the modified slab bed view factor and the hemispherical bolometer measurements depends heavily on I_B through $\widehat{E_f}$ and the flame length. An alternative simplistic model for the radiative flux was determined from a regression on I_B. The model was

$$q_r = \frac{a\alpha I_B}{\eta},$$

where $\hat{a} = 0.0160$ (see Figure 2.5). Note that the good correlation is due, in part, to the presence of α in both q_r and in the right-hand side of the equation.

2.7 Convective heat transfer coefficient $\hbar$

In modelling $\hbar$ we used the Reynolds-Nusselt number dependence, estimating c and m from regression, and trying various measurements of temperature to determine the Reynolds, Nusselt and Prandtl numbers. The Reynolds and Nusselt numbers were based on the particle diameter, which could be approximated by $\frac{4}{s}$. We tried several different windspeeds in the Reynolds-Nusselt correlation, including the average surface windspeed recorded by the velocity probe during the period of convective transfer, and a formula by Raupach giving the windspeed reduced by the entrained wind (Raupach 1990). The best correlation was given by simply using the ambient windspeed. This is fortunate as it does not involve further submodelling. The temperature which gave the best dependence was the air temperature at fuel ignition, $T_{a_{ig}}$.

The constant c was fuel dependent. In addition there was a slight packing ratio correction, giving a smaller heat transfer coefficient for more heavily packed beds, possibly due to reduced convectional transfer caused by decreased wind velocity close to the fuel surface. The Reynolds-Nusselt correlation for wind-aided fires was found to be

$$N_u = c\beta^n R_e^m,$$

where c was estimated as 0.011 for regular excelsior, 0.025 for coarse excelsior, 0.028 for sticks, and 0.007 for pine needles. m was estimated as 0.71, and n as -0.40. The R^2 value was 0.76. The Prandtl number is virtually constant over the range of temperatures measured, and was not included in the correlation.

The packing ratio had only a marginally significant effect in the regression of N_u on R_e. An alternative regression equation without the packing ratio dependence was

$$N_u = cR_e^m,$$

where c was estimated as 0.071 for regular excelsior, 0.170 for coarse excelsior, 0.203 for sticks, and 0.039 for pine needles. m was estimated as 0.60. The R^2 value for this regression was 0.74, which is not much worse. See Figure 2.6 for a plots of the relationship of N_u and R_e, and the fit of the model.

2.8 Temperature-time area

We needed to model $\int_0^\infty (T_a - T)dX$. Our estimates of this area were taken from the point where $T_a - T > 5°\text{K}$ to avoid overestimates due to thermocouples not reading exactly the same under identical conditions. The assumption was made in the submodel that the fuel temperature rises very little relative to the air temperature in the few seconds where convective heat transfer is important. A similar assumption was made by Hottel *et al.* (1965). Thus we can approximate $\int_0^\infty (T_a - T)dX$ as $L_c \times (T_{a_{ig}} - 500)$ where 500°K is an estimate of the fuel temperature over the length L_c. L_c can be referred to as the 'convection length' (see Figure 2.7). (see also Baines 1990). It is necessary, therefore to model the convection length L_c and the air temperature at ignition $T_{a_{ig}}$.

More complicated models of the air temperature profile, and hence $\int_0^\infty (T_a - T)\, dX$, using Gaussian or exponential decay (see §1.3(ii)) will be investigated later.

2.9 Air temperature at ignition, $T_{a_{ig}}$

The air temperature at ignition was measured as the average air temperature from a quarter of a second before, to a quarter of a second after the fuel temperature reached $520K$. It was found to be strongly correlated with the heat sink terms $\rho_b \eta Q_{ig}$. The regression model used was of the form

$$T_{a_{ig}} = a + b\,(\rho_b \eta Q_{ig})$$

where $\hat{a} = 1050$ and $\hat{b} = -0.0124$. The correlation, however, was poor, with $R^2 = 0.20$ (see Figure 2.8). We intend to develop a physically-based model for $T_{a_{ig}}$ which should give a better correlation.

2.10 Convection length L_c

It seems natural that the convection length depends on the balance of windspeed and fire intensity. It was found to be strongly related to the Froude

number in flame height, which is the ratio of inertia to bouyancy. Convection length intuitively should also depend on the flame shadow $S_f = L \sin \phi_f$ (see Figure 2.9 below).

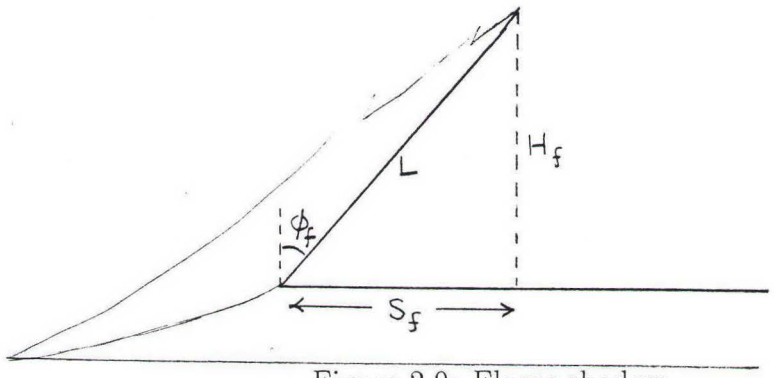


Figure 2.9: Flame shadow

It can be seen from Figure 2.10 that the convection lengths for the sticks were a lot longer than those for the fine fuel. This is caused by the much larger areas between the air and fuel temperature profiles for the stick fires. This may be because the stick thermocouples are buried deeper than the thermouples in the fine fuel, and are not giving a good estimate of surface temperature. Only the sticks with thermocouples in the front and rear are included in Figure 2.10, as it was thought that the convectional transfer of heat was not being measured properly by the thermocouples at the centre. The sticks with thermocouples at the rear tended to have smaller areas than the sticks with thermocouples at the front, but even they had relatively larger areas than the fine fuel.

Although the area can be seen to be larger for the sticks (which have much lower surface-area to volume ratios) attemps to incorporate a fuel diameter dependence, or a drag dependence of the form $s\beta$, for the fine fuel, were not successful. And since we had reservations about the measurements of the convection area for the stick fuels, we used only the Froude number and the flame shadow to predict convection length until we had made further investigation of the temperature-time areas for the stick fires.

We modelled convection length for fine fuel as

$$L_c = a + b\, F_r S_f,$$

where $\hat{a} = 0.0391$ and $\hat{b} = 0.1592$ ($R^2 = 0.23$). See Figure 2.10 for a plot of the relationship and the fit of the model.

This completed the submodelling of the heat transfer terms for the model using the modified slab bed view factor and the hemispherical bolometer measurements. An energy balance for the alternative model using volume heating and variable flame temperature with height has been done, but submodelling of resulting terms has not yet been attempted. Note, however that the models for flame dimensions and temperature-time area (which includes convection length and air temperature at ignition) will be relevant for this alternative model.

The energy balance using the submodels described above is given in Figure 2.11. It can be seen that the submodelling overpredicts the propagating flux for the regular excelsior, but does reasonably well for the other fuels. To investigate which submodels are causing a problem we looked at the radiative flux terms only. We plotted the measured propagating flux I_P against the radiative flux with view factor calculated with measured flame dimensions and the measured radiative emissive flux from the bolometer. The resulting plot is shown in Figure 2.12.

In the following we use the terms "measured values" q_r and q_c to refer to the radiative and convective fluxes determined partly by measurement and partly by energy balance of (1.27) and (1.28). The "modelled values" $\widehat{q_r}$ and $\widehat{q_c}$ refer to the empirically submodelled radiative and convective fluxes.

Plots of measured versus modelled terms for radiative and convective heat transfer are given in Figures 2.13 and 2.14. Figure 2.13 shows that the regular excelsior fires are slightly overpredicted by the radiative submodels. The fluxes are underpredicted for the stick and needle fires, while the predictions for the excelsior fires are on average correct, but extremely variable.

Figure 2.15 gives a flux balance for all the fires in our data base (many of which didn't have sufficient instrumentation to include in the determination of submodels). This shows a distinct 'banana shape', indicating underprediction for small values of the propagating flux, I_P, and overprediction for large values of I_P.

2.11 Estimating the spread rate

Having submodelled the radiative and convective fluxes it is then necessary to determine the predicted value of the spread rate R and compare it with the measured spread rate. Since R appears on both sides of the prediction equation based on (1.27)

$$I_P = \widehat{q_r} + \widehat{q_c}$$

(through the submodels dependence on Bryam's intensity) it was necessary to use iterative methods to obtain estimates of R. The results, using the

same submodels as in the flux balance in Figure 2.11, are shown in Figure 2.16.

It can be seen that although the submodels for propagating flux give reasonable predictions for the propagating flux I_P, they give very poor predictions for spread rate for several of the fires. In particular they give severe over-predictions for the regular excelsior fires. The poor predictions may relate to the strong dependence of the radiative flux on I_B discussed above. Since I_B is linearly related to R the spread rate is poorly determined by the submodelled equation when the convective flux is small. If this is still a problem when the submodelling is done for the volume heating model (and preliminary analysis suggests it may be) we will need to consider submodels based on (1.28) instead of (1.27) .

2.12 Field data

Figures 2.17 and 2.18 show the submodelled equation applied to field data to determine the propagating flux I_P. The fit is good both for the grass data (Sneeuwjagt & Frandsen 1977) and the red pine needle data (VanWagner 1963). The spread rates were then predicted and compared against the observed spread rates in Figures 2.19 and 2.20. It can be seen that the predictions are much worse than the predictions of propagating flux. However, the propagating flux predictions use the measured spread rate. In the case of Sneeuwagt's cured grass, for example, the fire with the highest spread rate has very similar parameters to the fire with second highest spread rate (the only different being a slightly higher fuel loading). The measured spread rate of the first fire seems very high compared to that of the second fire, so a poor prediction of spread rate may not necessarily mean that the model is predicting badly.

2.13 Further work

Work on submodels for the volume heating model is planned shortly. Submodelling needs to be improved, and based if possible on phyical considerations. In particular the parameters for the flame model need to determined and the model tested against laboratory and field data. If it is not possible to obtain good rate of spread predictions from (1.27) then (1.28) will be used for submodelling.

In view of the comment above about estimates of convective heat transfer and effective flame length being dependent on burning conditions, and

because every submodel reduces the accuracy of the predictions, it may be necessary to use the submodelling to determine the form of the relationships required, and then fit the parameters of the submodel to obtain as close an agreement as possible with the measured propagating flux.

To predict spread rate in natural fuels it will then be necessary to determine modifications of the models to include the effects of mixed fuel sizes, live fuel and slope.

References

Albini, F.A. (1981). A model for the wind-blown flame from a line fire. *Combust. Flame*, **43**, 155–174.

Albini, F.A. (1985). A model for fire spread in wildland fuels by radiation. *Comb. Sci. and Technol.*, **42**, 229–258.

Albini, F.A. (1986). Wildland fire spread by radiation — a model including fuel cooling by convection. *Comb. Sci. and Technol.*, **45**, 101–113.

Baines, P. (1990). Physical mechanisms for the propagation of surface fires. *Mathematical and Computer Modelling*, **12**, 83–94.

Brown, A.A. & Davis, K.P. (1973). Forest fire: control and use. McGraw-Hill Inc., 2nd Ed., 686pp.

Butler, B.W. (1993). Experimental Measurements of Radiant Fluxes from Simulated Wildfire Flames, presented at 12th Conference on Fire and Forest Meteorolory, October 26–28, 1993, Jekyll Island, GA, pp. 104–111. SAF Publication 94–02

Catchpole E.A. & Catchpole W.R. (1991) Modelling moisture damping for fire spread in a mixture of live and dead fuels. *Int. J. Wildland Fire*, **1**, 101–106.

Catchpole, E.A., Catchpole W.R. & Rothermel, R.C. (1993) Fire behavior experiments in mixed fuel complexes. *Int. J. Wildland Fire*, **3**, 45–57.

de Mestre, N.J., Catchpole, E.A., Anderson, D.H. and Rothermel, R.C. (1989). Uniform propagation of a planar fire front without wind. *Comb. Sci. and Technol.* **65**, 231–244.

Dunlap, F. (1912). The specific heat of wood. USDA Forest Service, Bulletin 110.

Frandsen, W.H. (1973). Effective heating of fuel ahead of spreading fire. USDA For. Serv. Res. Pap. INT-140, Intermt. For. and Range Exp. Stn., Ogden, Ut., USA, 16pp.

Hamilton & Morgan (1952). Radiant-interchange configuration factors. National Aeronautics and Space Administration, Tech. Note 2836.

Hottel, H.C., Williams, G.C. and Steward, F.R. (1965). Modelling of fire-spread through a fuel bed. *Tenth Symp. (Internat.) on Combustion*, 997–1007. The Combustion Institute.

Incropera, F.P. and de Witt, D.P. (1990). *Fundametals of Heat and Mass Transfer*, 3rd ed. Wiley.

Monteith, J.L. and Unsworth, M.H. (1990). *Principles of Environmental Physics*, 2nd ed. Edward Arnold, London.

Nelson, R.M. and Adkins, C.W. (1986). Flame characteristics of wind-driven surface fires. *Can. J. For. Res.*, **16**, 1293–1300.

Raupach, M.R. and Shaw, R.H. (1982). Averaging procedures for flow within vegetation canopies. *Boundary-Layer Meteorology*, **22**, 79-90.

Raupach, M.R. (1990). Similarity analysis of the interaction of bushfire plumes with ambient winds. Proceedings of the workshop on bushfires: Meteorology and Dynamics. *Mathematical & Computer Modelling*, **13**, 113–121.

Rothermel, R.C. (1971). An examination of radiation's role in rate of fire spread in wildland fuels. M.Sc. thesis, Colorado State University, Fort Collins, Colorado.

Rothermel, R.C. (1972). A mathematical model for predicting fire spread in wildland fuels. USDA For. Serv. Res. Pap. INT–115, Intermt. For. and Range Exp. Stn. Ogden, Utah, USA, 40pp.

Siegel, R. and Howell, J.R. (1972). *Thermal Radiation Heat Transfer.* McGraw-Hill.

Sneeuwjagt, R.J. and Frandsen, W.H. (1977). Behavior of experimental grass fires vs. predictions based on Rothermel's fire model. *Can. J. For. Res.*, **7**, 357–367.

Thomas, P.H. (1963). The size of flames from natural fires. *Ninth Symp. (Internat.) on Combustion*, 844–858. The Combustion Institute.

Thomas, P.H. (1967). Some aspects of the growth and spread of fire in the open. *Forestry*, **40**, 139–164.

Van Wagner, C.E. (1963). Prescribed burning experiments: red and white pine. Can. Dep. For., For. Res. Branch, Ottawa, Ont. Pub. No. 1020. 27p.

Appendix A

Glossary of notation

$\alpha = s\beta/4$	decay constant for radiation through the fuel bed
β	packing ratio of fuel bed = volume of fuel per unit volume of fuel bed
ϵ_b	combustion interface emissivity
ϵ_f	flame emissivity
η	the effective fraction of the fuel raised to ignition temperature during the preheating process
ϕ_f	flame angle to vertical
ν	kinematic viscosity of gas (air)
$\rho_b = \beta\rho_p$	bulk density of fuel = mass of fuel per unit volume of fuel bed
ρ_p	density of a single fuel particle
σ_B	Stefan-Boltzman constant
b	effective flame height multiplier
c_p	specific heat of dry fuel
c_w	specific heat of water
c^*	'average specific heat' of fuel
D_f	flame depth at base of flame
$E_f = \epsilon_f\sigma_B T_f^4$	flame emissive power
F_r	Froude number
h	the depth of the fuel bed
$\hbar$	convective heat transfer coefficient

h_c	fuel low heat content
H_f	flame height
I_B	fireline intensity
$I_P = R\rho_b\eta Q_{\text{ig}}$	propagating flux
k	thermal conductivity of gas (air)
L_f	flame length
L_c	convection length
$\mathcal{L}$	latent heat of water
m	moisture content of fuel = mass of water per unit mass of fuel
$N_u = \hbar L/k$	Nusselt number
q	rate of heat inflow into unit volume of the fuel bed
q_b	radiative heating rate from the combustion (ember) zone
q_c	convective heating rate
q_f	radiative heating rate from the flames
q_ℓ	cooling rate
Q	quantity of heat per unit mass of fuel
Q_{ig}	quantity of heat required to raise unit mass of fuel to ignition temperature
$R_e = U_0 L/\nu$	Reynolds number
s	surface area to volume ratio of a single fuel particle
$S_f = L\sin\phi_f$	flame shadow
T	fuel particle temperature
T_f	flame temperature
T_{ig}	Ignition temperature
T_∞	ambient temperature
U	wind speed
U_0	wind speed at surface of or within fuel bed
$w = \rho_b h$	total fuel loading per unit area of the fuel bed
w_a	actual fuel load consumed during combustion

Appendix B

Energy balance for a single particle

We derive here the rate of radiation from the flame absorbed by a single particle on the fuel surface. We assume that the particle is cylindrical and oriented horizontally, directly across the fuel bed: that is, parallel to the flame (see figure B.1). This orientation is of special interest because the instrumented pine needles were oriented in this way. However it is a simple matter to redo the calculation for any other orientation.

We use a coordinate system (X, y, z) moving with the flame, whose origin is at the base of the flame and, in the case of a finite-width flame, at the centre of the flame. The fuel particle is located on the fuel surface a distance X ahead of the flame, at point Q with position vector $(X, 0, 0)$. We consider a ray, from a point $P = (z \tan \phi_f, y, z)$ on the flame surface at height z above the fuel bed, onto the particle. First note that

$$\overrightarrow{PQ} = (X - z \tan \phi_f, -y, -z)$$

and that the unit normal to the flame at P is

$$\mathbf{n} = (\cos \phi_f, 0, -\sin \phi_f),$$

and so the angle θ_1 between the ray and the normal satisfies

$$\cos \theta_1 = \frac{\mathbf{n}.\ \overrightarrow{PQ}}{\| \overrightarrow{PQ} \|} = \frac{(X - z \tan \phi_f) \cos \phi_f + z \sin \phi_f}{r} = \frac{X \cos \phi_f}{r},$$

where

$$r = \| \overrightarrow{PQ} \| = \sqrt{(X - z \tan \phi_f)^2 + y^2 + z^2}.$$

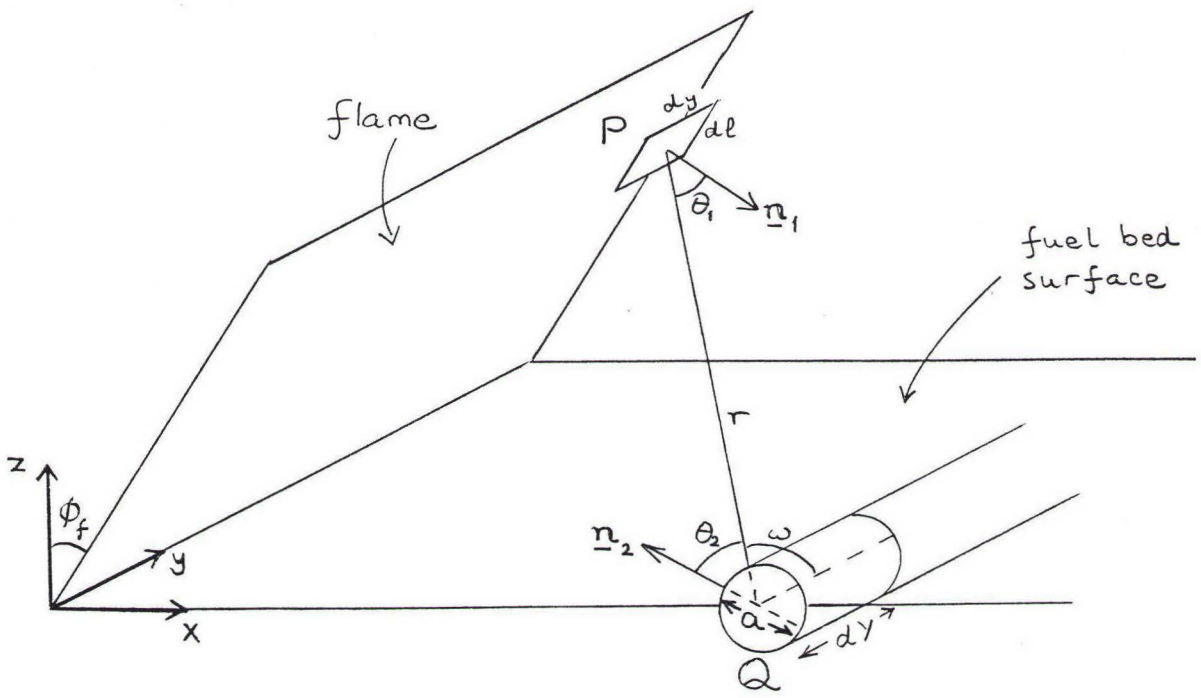


Figure B.1: Radiation from the flame onto a single particle.

The unit vector along the particle is $\overrightarrow{QR}$= $(0,1,0)$, and so the angle ω between the ray and the particle satisfies

$$\cos\omega = \frac{\overrightarrow{QP}\,.\,\overrightarrow{QR}}{\parallel \overrightarrow{QP} \parallel} = \frac{y}{r}.$$

Hence the angle θ_2 between the ray and the normal plane to the particle satisfies

$$\cos\theta_2 = \sin\omega = \frac{\sqrt{(X - z\tan\phi_f)^2 + z^2}}{r}.$$

Now consider a length dY of the particle at Q. The area of this segment, as seen from P, is $adY\cos\theta_2$, where a is the diameter of the cylinder. Hence the solid angle subtended at P is $adY\cos\theta_2/r^2$.

The intensity of radiation emitted per unit solid angle from a small element dA of the flame surface at P, in the direction $\overrightarrow{PQ}$, is

$$dI = \frac{E_f}{\pi} dA\cos\theta_1,$$

where $E_f = \sigma_B \epsilon_f T_f^4$ is the hemispherical flame emissive power at the point P, which in general will depend on the height z. Writing $dA = dy\,d\ell = dy\,dz/\cos\phi_f$, where $d\ell$ is measured along the flame (see figure B.1), this

becomes

$$dI = \frac{E_f}{\pi} \cos\theta_1 \frac{dy\,dz}{\cos\phi_f}.$$

We assume that the particle is radiatively black, so that it aborbs all radiation incident upon it. Thus the rate of absorption of radiation by the particle element at Q, from the flame element at P, is

$$\begin{aligned} dI &= \frac{E_f}{\pi} \cos\theta_1 \frac{dy\,dz}{\cos\phi_f} \frac{a dY \cos\theta_2}{r^2} \\ &= \frac{E_f}{\pi} \frac{X\cos\phi_f}{r} \frac{dy\,dz}{\cos\phi_f} \frac{a dY}{r^2} \frac{\sqrt{(X - z\tan\phi_f)^2 + z^2}}{r}. \end{aligned}$$

Hence the rate of absorption of radiation from the flame, per unit length of the particle, is

$$dE = E_{f,0} a J_f(X),$$

where $E_{f,0}$ is the flame emissive power at the base of the flame, and

$$J_f(X) = \frac{X}{\pi} \int_{z=0}^{H} \frac{E_f(z)}{E_{f,0}} \int_{y=-W}^{W} \frac{\sqrt{(X - z\tan\phi_f)^2 + z^2}}{r^4} dy\,dz,$$

where $r^2 = (X - z\tan\phi_f)^2 + y^2 + z^2 = c^2 + y^2$ say, and the flame is taken to be of height H and of width $2W$. The innermost integral is

$$\int_{y=-W}^{W} \frac{c}{(c^2 + y^2)^2} dy = \frac{1}{c^2} \left\{ \arctan\left(\frac{W}{c}\right) + \frac{cW}{c^2 + W^2} \right\}.$$

Hence

$$J_f(X) = \frac{X}{\pi} \int_{z=0}^{H} \frac{E_f(z)}{E_{f,0}} \frac{1}{c^2} \left\{ \arctan\left(\frac{W}{c}\right) + \frac{cW}{c^2 + W^2} \right\} dz, \qquad \text{(B.1)}$$

where $c^2 = (X - z\tan\phi_f)^2 + z^2$.

We now apply the conservation of energy to a unit length of the fuel particle, to derive the fundamental differential equation analagous to equation (1.21). First note that the volume of this segment is $\pi a^2/4$, and its surface area is πa. As before, we assume that only a fraction η of the particle is involved in the preheating process. The equation is thus

$$-R\frac{\pi a^2}{4} \rho_p \eta c^* \frac{dT}{dX} = E_{f,0}\, a\, J_f(X) + \pi a \hbar(X)\big(T_a(X) - T(X)\big). \qquad \text{(B.2)}$$

This can be rewritten in terms of the particle's surface-area to volume ratio $s = 4/a$ as

$$-R\rho_p \eta c^* \frac{dT}{dX} = \frac{E_{f,0}}{\pi} s\, J_f(X) + s\hbar(X)\big(T_a(X) - T(X)\big). \qquad \text{(B.3)}$$

Note that this equation is very similar to (1.21). The similarity is more apparent if we divide throughout (1.21) by the packing ratio β to obtain

$$-R\rho_p\eta c^* \frac{dT}{dX} = \beta^{-1} q_f(X, L, \phi_f) + s\hbar(X)(T_a(X) - T(X)). \qquad \text{(B.4)}$$

It is clear that the difference, if any, resides solely in the radiative heating term q_f. Expressions for q_f for the various fuel bed models are derived in Appendix C.

Appendix C

Radiation absorption at the fuel surface

C.1 Slab bed and modified slab bed

We consider the same situation as in Appendix B, except that here the fuel bed surface is modelled as a solid. Thus we consider the radiation from an element dA_1 at P on the flame surface to an element dA_2 at Q on the fuel bed surface (see figure C.1).

From standard theory (see e.g Siegel and Howell equation 7.77), the rate of radiative transfer is

$$dI = \frac{E_f}{\pi} \frac{\cos\theta_1 \cos\theta_2}{r^2} dA_1 dA_2, \tag{C.1}$$

where θ_1 and θ_2 are the angles between the ray $\overrightarrow{PQ}$ and the normals to the surfaces. From figure C.1 we have that $\overrightarrow{PQ} = (X - z\tan\phi_f, -y, -z)$, and the normal to the flame surface is $\mathbf{n}_1 = (\cos\phi_f, 0, -\sin\phi_f)$, as in Appendix B, so that

$$\cos\theta_1 = \frac{X\cos\phi_f}{r},$$

where

$$r = \| \overrightarrow{PQ} \| = \sqrt{(X - z\tan\phi_f)^2 + y^2 + z^2}.$$

Also the normal to the fuel bed surface is $\mathbf{n}_2 = (0, 0, 1)$, and so

$$\cos\theta_2 = \frac{\mathbf{n}_2 . \overrightarrow{QP}}{r} = \frac{z}{r}.$$

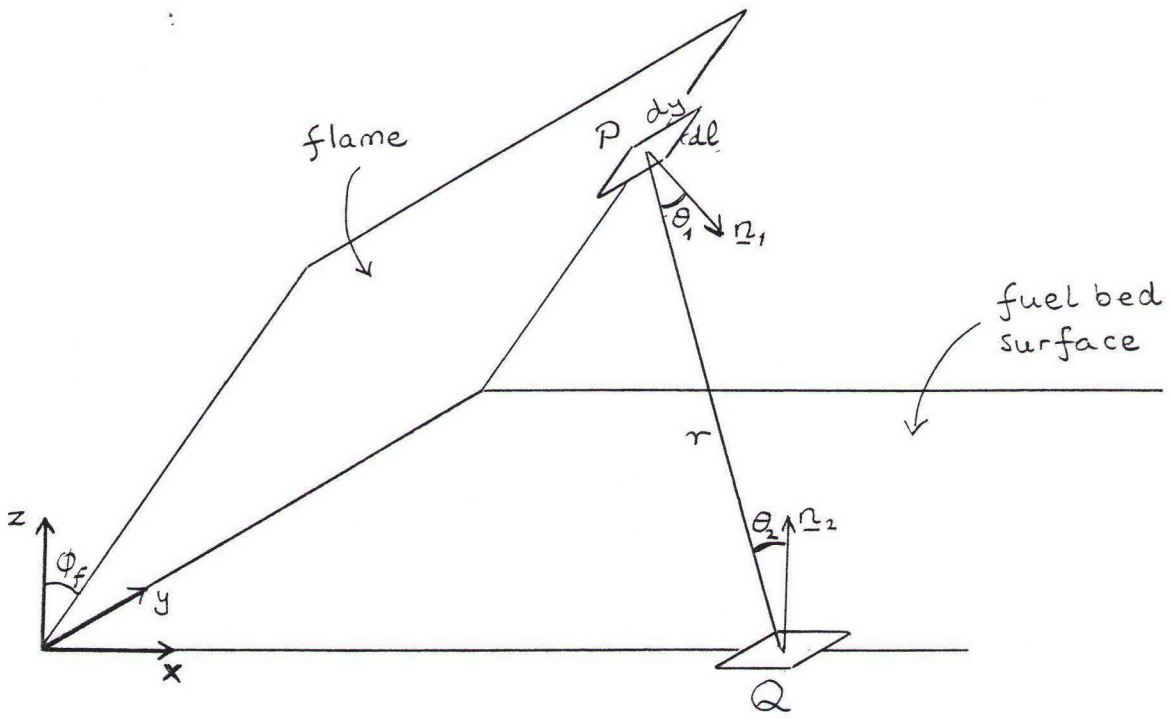


Figure C.1: Radiation from the flame to the fuel bed surface.

As in Appendix B, $dA_1 = dy\,dz/\cos\phi_f$, and so the rate of radiation from dA_1 which is absorbed by the fuel bed at Q, is

$$dI = \frac{E_f}{\pi}\frac{(X\cos\phi_f/r)(z/r)}{r^2}\frac{dy\,dz}{\cos\phi_f} = \frac{E_f}{\pi}\frac{Xz}{r^4}dy\,dz$$

per unit surface area of the fuel bed. We now consider the radiation dE from a horizontal strip on the flame surface, at height z above the fuel bed and of width $d\ell = dz/\cos\phi_f$, by integrating dI with respect to y. This gives

$$dE = \frac{E_f}{\pi}Xz\int_{y=-W}^{W}\frac{dy}{r^4}\,dz = \frac{E_f}{\pi}\frac{Xz}{c^3}\left\{\arctan\left(\frac{W}{c}\right) + \frac{cW}{c^2+W^2}\right\}dz,$$

where $c = \sqrt{(X - z\tan\phi_f)^2 + z^2}$. Hence the total radiative flux falling on the fuel bed surface at Q is $E_{f,0}J_f(X)$, where

$$J_f(X) = \frac{X}{\pi}\int_{z=0}^{H}\frac{E_f(z)}{E_{f,0}}\frac{z}{c^3}\left\{\arctan\left(\frac{W}{c}\right) + \frac{cW}{c^2+W^2}\right\}dz. \qquad \text{(C.2)}$$

In the special case where the flame temperature and emissivity are assumed constant over the whole flame surface, $J_f(X)$ is the view factor between the flame surface and dA_2. From Hamilton and Morgan (1952), we have

$$J_f(X) = \frac{1}{\pi}\left\{\frac{W\sin\phi_f}{V_2}\left[\arctan\left(\frac{L - X\sin\phi_f}{V_2}\right) + \arctan\left(\frac{X\sin\phi_f}{V_2}\right)\right] +$$

$$+ \quad \arctan\left(\frac{W}{X}\right) - \frac{X - L\sin\phi_f}{V_1} \arctan\left(\frac{W}{V_1}\right)\Bigg\} \tag{C.3}$$

where

$$V_1 = \sqrt{(X - L\sin\phi_f)^2 + (L\cos\phi_f)^2}, \qquad V_2 = \sqrt{W^2 + (X\cos\phi_f)^2}.$$

Note that for an infinitely wide fire front ($W \to \infty$), then, in general we get from (C.2)

$$J_f(X) = \frac{X}{2}\int_{z=0}^{H} \frac{E_f(z)}{E_{f,0}} \frac{z}{c^3}\, dz \tag{C.4}$$

while for a constant temperature flame we get from (C.3) or (C.4)

$$J_f(X) = \frac{1}{2}\left(1 - \frac{X - L\sin\phi_f}{V_1}\right). \tag{C.5}$$

For the modified slab bed model, we assume that rate of radiation absorption by a volume element on the fuel bed surface, of top surface area dA_2 and thickness dz, is equal to αdz times the radiation falling on dA_2. This gives a rate of radiation absorption per unit volume of fuel bed as

$$q_f(X) = \alpha E_{f,0} J_f(X), \tag{C.6}$$

where $J_f(X)$ is given by one of the above equations.

C.2 Volume heating

The fuel bed is modelled as a collection of randomly oriented, radiatively black particles. Consider a beam of radiation from a small region dA_1 on the flame surface to a small cylindrical volume element on the surface of this bed (see figure C.2). The rate of radiation from dA_1 falling onto this volume is dI, as given by (C.1), except that now $\theta_2 = 0$. Each ray in this beam will meet a fuel particle and be absorbed with probability αdr, where[1] $\alpha = s\beta/4$, and so the rate of radiative energy absorbed by the volume element is

$$dE = \alpha\, dI\, dr = \alpha \frac{E_f}{\pi} \frac{\cos\theta_1}{r^2}\, dA_1\, dV,$$

where $dV = dA_2\, dr$ is the volume of the fuel element.

[1]This equation is correct for convex fuel particles. We ignore the small error for non-convex particles.

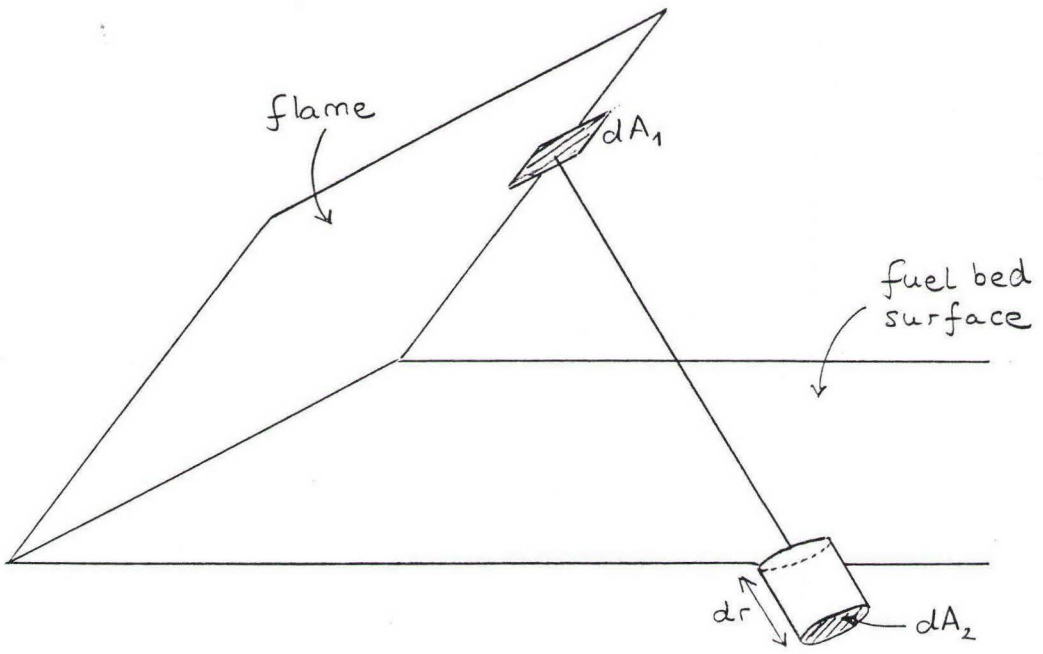


Figure C.2: Radiation from the flame to a volume element on the fuel bed surface.

Thus the rate of energy absorbed by the fuel bed, per unit volume of fuel bed, from the flame element dA_1 is

$$\frac{dE}{dV} = \alpha \frac{E_f}{\pi} \frac{X \cos\phi_f}{r^3} \, dA_1 = \alpha \frac{E_f}{\pi} \frac{X}{r^3} \, dy \, dz.$$

Thus the total rate of radiative energy from the flame, absorbed per unit volume of the fuel bed, is $\alpha E_{f,0} \, J_f(X)$, where

$$\begin{aligned} J_f(X) &= \frac{X}{\pi} \int_{z=0}^{H} \frac{E_f(z)}{E_{f,0}} \int_{y=-W}^{W} \frac{dy}{r^3} \, dz \\ &= \frac{2XW}{\pi^2} \int_{z=0}^{H} \frac{E_f(z)}{E_{f,0}} c^2 \sqrt{c^2 + W^2} \, dz, \end{aligned}$$

where

$$c^2 = (X - z \tan\phi_f)^2 + z^2.$$

In the special case where E_f is constant over the flame surface this reduces to

$$\begin{aligned} J_f(X) &= \frac{2}{\pi} \left\{ \arctan\left(\frac{W(L - X\sin\phi_f)}{X\cos\phi_f \sqrt{(L\cos\phi_f)^2 + W^2 + (X - L\sin\phi_f)^2}} \right) \right. \\ &\quad \left. + \arctan\left(\frac{W\tan\phi_f}{\sqrt{W^2 + X^2}} \right) \right\}. \end{aligned} \tag{C.7}$$

A special case of this formula, with $\phi_f = 0$, was given in de Mestre *et al* (1989).

Captions for figures

Fig 1.6. Profile of average temperature versus height in the flame.

Fig 1.7. Method of obtaining $\hbar$ and the flame length modifier from equations (1.27) and (1.28).

Fig 1.8. Air and fuel temperature versus time before the fire-front arrives, showing predicted fuel temperature from (1.21) for a given $\hbar$ and flame length modifier.

Fig 1.9. Measured propagating flux versus sum of radiative and convective fluxes for (1.27) (with the modified slab bed model), using the values of $\hbar$ and flame length modifier obtained in the iterative balance procedure.

Fig 1.10. Measured propagating flux versus sum of radiative and convective fluxes for (1.27) (with volume heating model, and a linear flame temperature profile), using the values of emissivity and $\hbar$ obtained from a least squares fit to (1.21).

Fig 2.1. Flame length versus Byram's intensity, and fit of regression model.

Fig 2.2. Tan of flame angle versus Froude number, and fit of regression model.

Fig 2.3. Flame height versus IB/U, and fit of regression model.

Fig 2.4. Radiative emissive flux versus flame depth, flame length and Byram's Intensity, and fit of regression model using IB.

Fig 2.5. Fit of regression model for radiative flux in terms of IB and α.

Fig 2.6. Correlation between Nusselt and Reynolds number (using free-stream velocity and air temperature at ignition in the Reynolds number) and fit of model for $\hbar$ based on this correlation.

Fig 2.7. Air and fuel temperature profiles ahead of the fire showing area approximated to $\int_0^\infty (T_a - T)dX$, and resulting convection length L_c.

Fig 2.8. Air temperature at ignition versus heat sink terms, and fit of regression model.

Fig 2.10. Convection length versus product of Froude number and flame shadow for fine fuels, and fit of regression model.

Fig 2.11. Measured versus predicted propagating flux for modified slab bed model using submodelled terms in (1.27).

Fig 2.12. Measured propagating flux versus submodelled radiative flux for modified slab bed model.

Fig 2.13. Measured versus predicted radiative flux for modified slab bed.

Fig 2.14. Measured versus predicted convective flux for modified slab bed.

Fig 2.15. Measured versus predicted propagating flux for all the laboratory data, showing underprediction for low propagating flux, and overprediction for high propagating flux.

Fig 2.16. Observed versus predicted spread rates corresponding the predicted propagating fluxes in Fig 2.11.

Fig 2.17. Observed versus predicted propagating for grassland data.

Fig 2.18. Observed versus predicted propagating flux for red pine needle data.

Fig 2.19. Observed versus predicted spread rate for grassland data.

Fig 2.20. Observed versus predicted spread rate for red pine data.

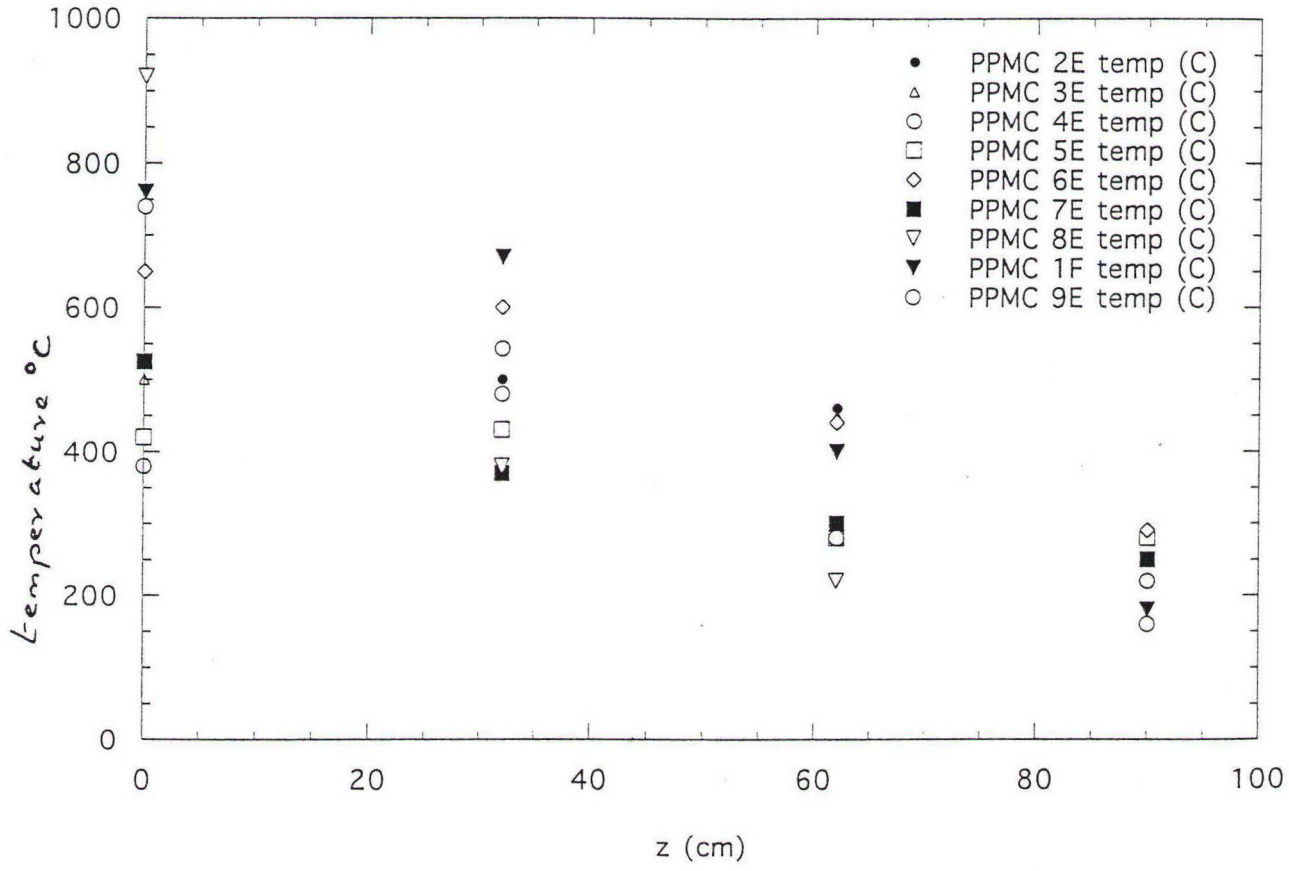
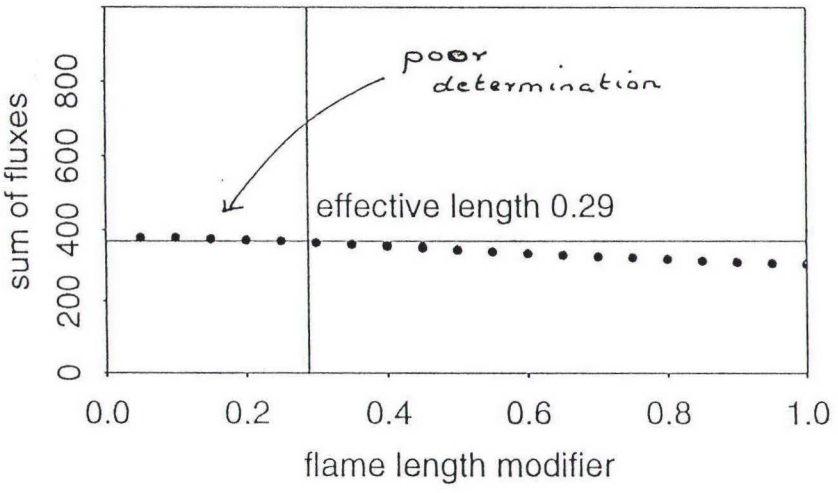
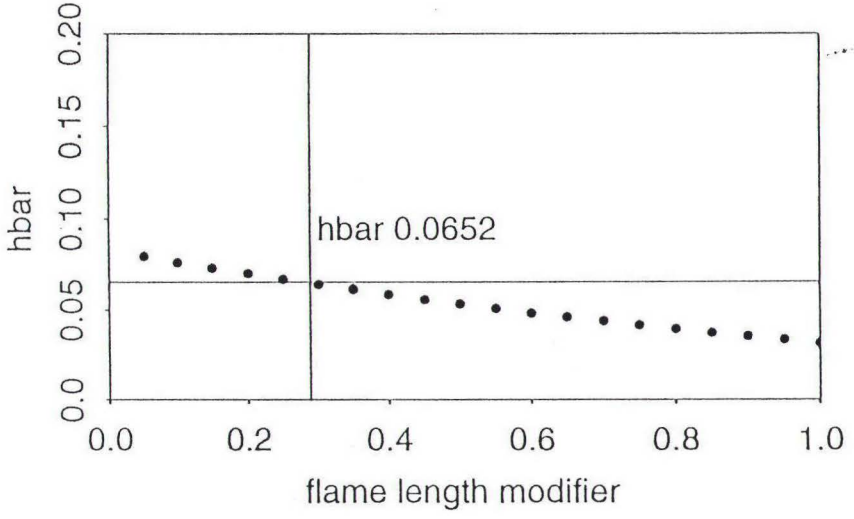

1000
800
600
400
200
0
Temperature °C
0
20
40
60
80
100
z (cm)
PPMC 2E temp (C)
PPMC 3E temp (C)
PPMC 4E temp (C)
PPMC 5E temp (C)
PPMC 6E temp (C)
PPMC 7E temp (C)
PPMC 8E temp (C)
PPMC 1F temp (C)
PPMC 9E temp (C)

Figure 1.6

EXSC62 rung 3 NACA factor





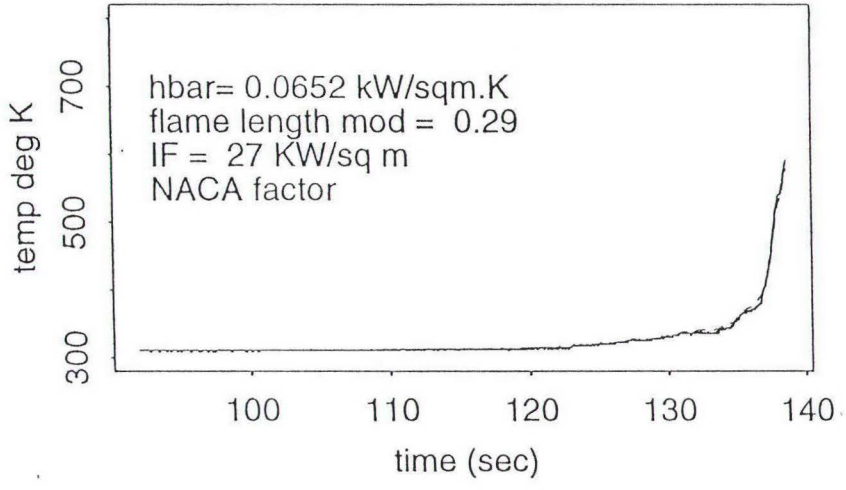


Figure 1.7

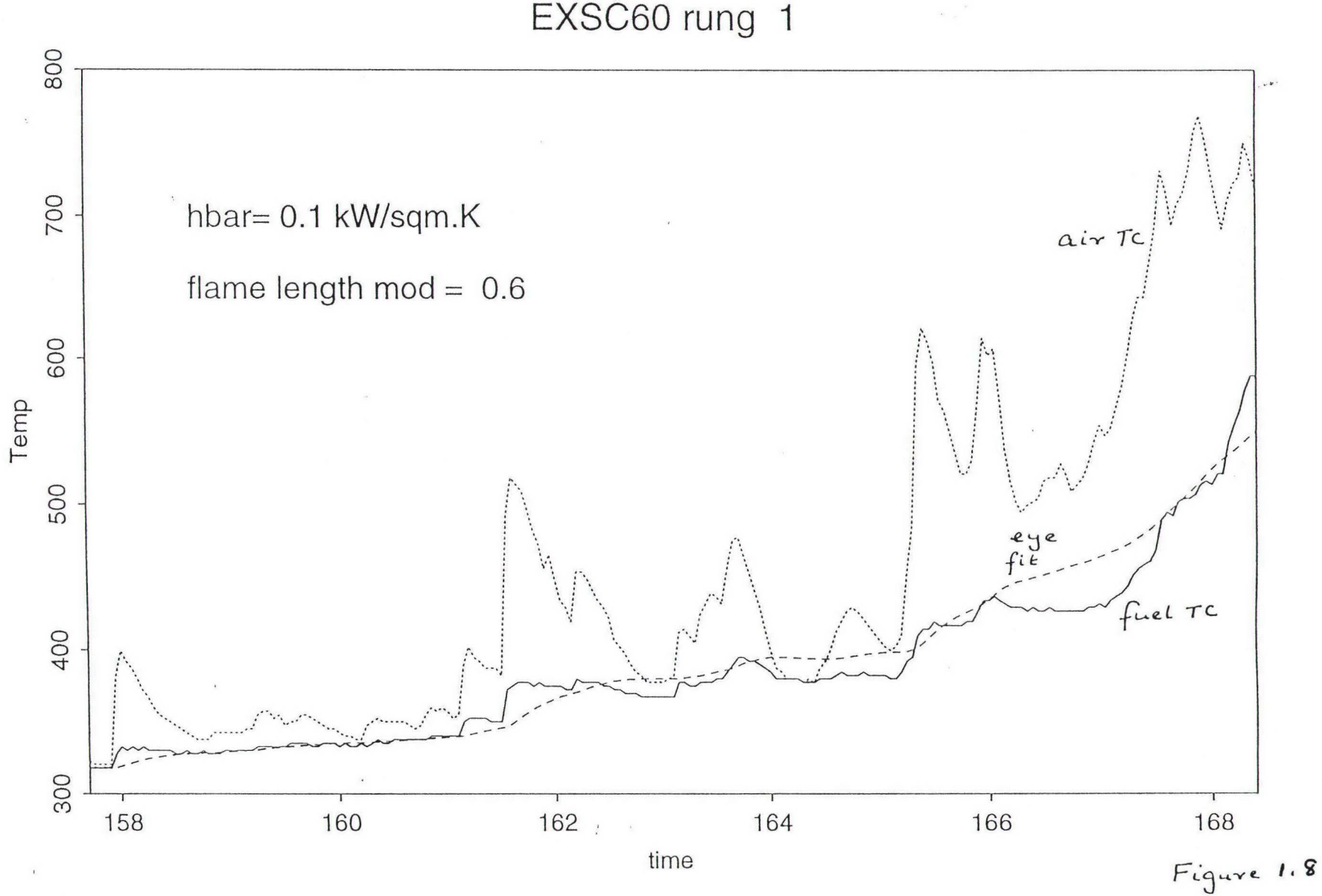

EXSC60 rung 1
hbar= 0.1 kW/sqm.K
flame length mod = 0.6
air Tc
eye fit
fuel TC
Temp
time
300
400
500
600
700
800
158
160
162
164
166
168

Figure 1.8

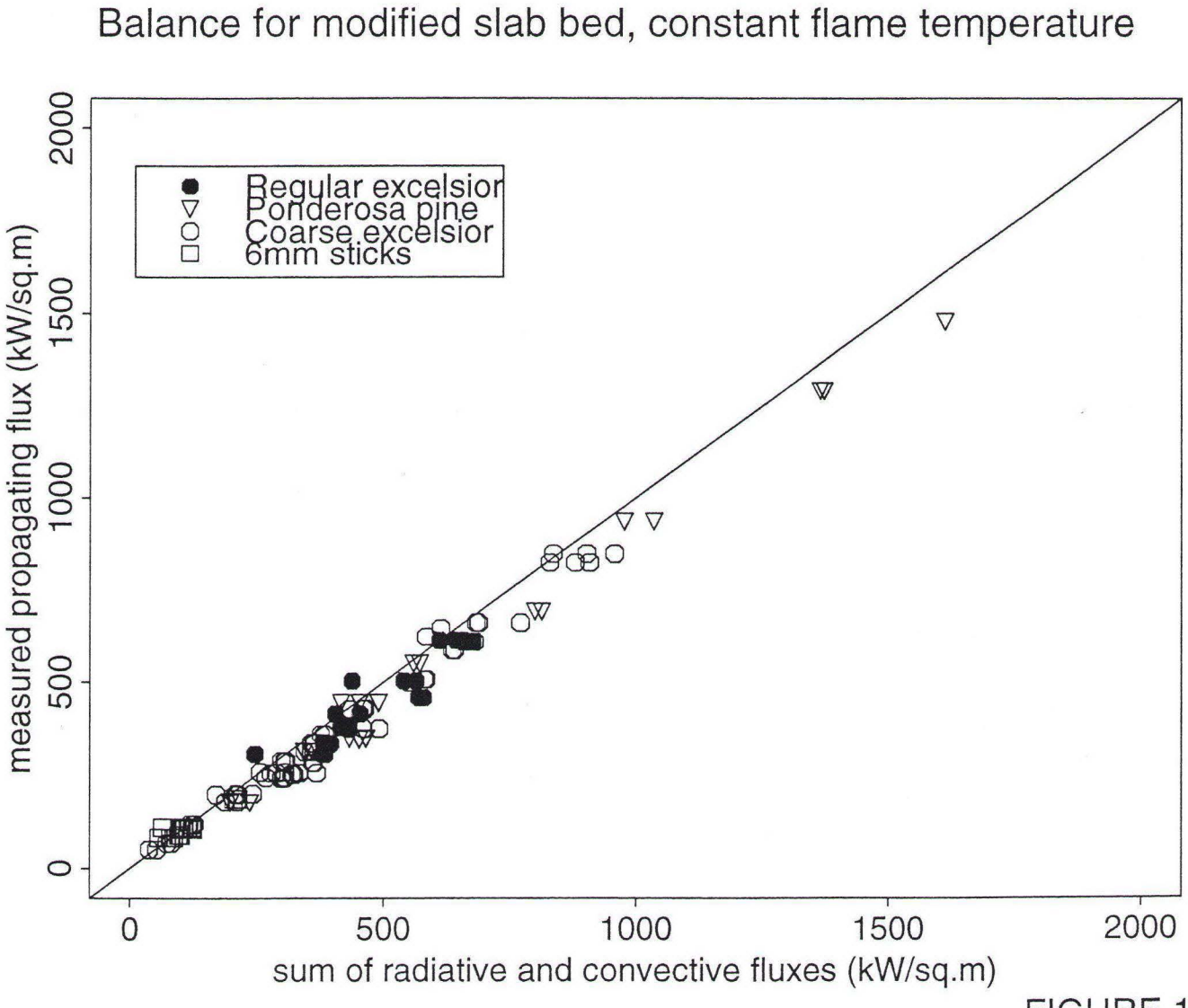

Balance for modified slab bed, constant flame temperature
Regular excelsior
Ponderosa pine
Coarse excelsior
6mm sticks
measured propagating flux (kW/sq.m)
0
500
1000
1500
2000
sum of radiative and convective fluxes (kW/sq.m)

FIGURE 1.9

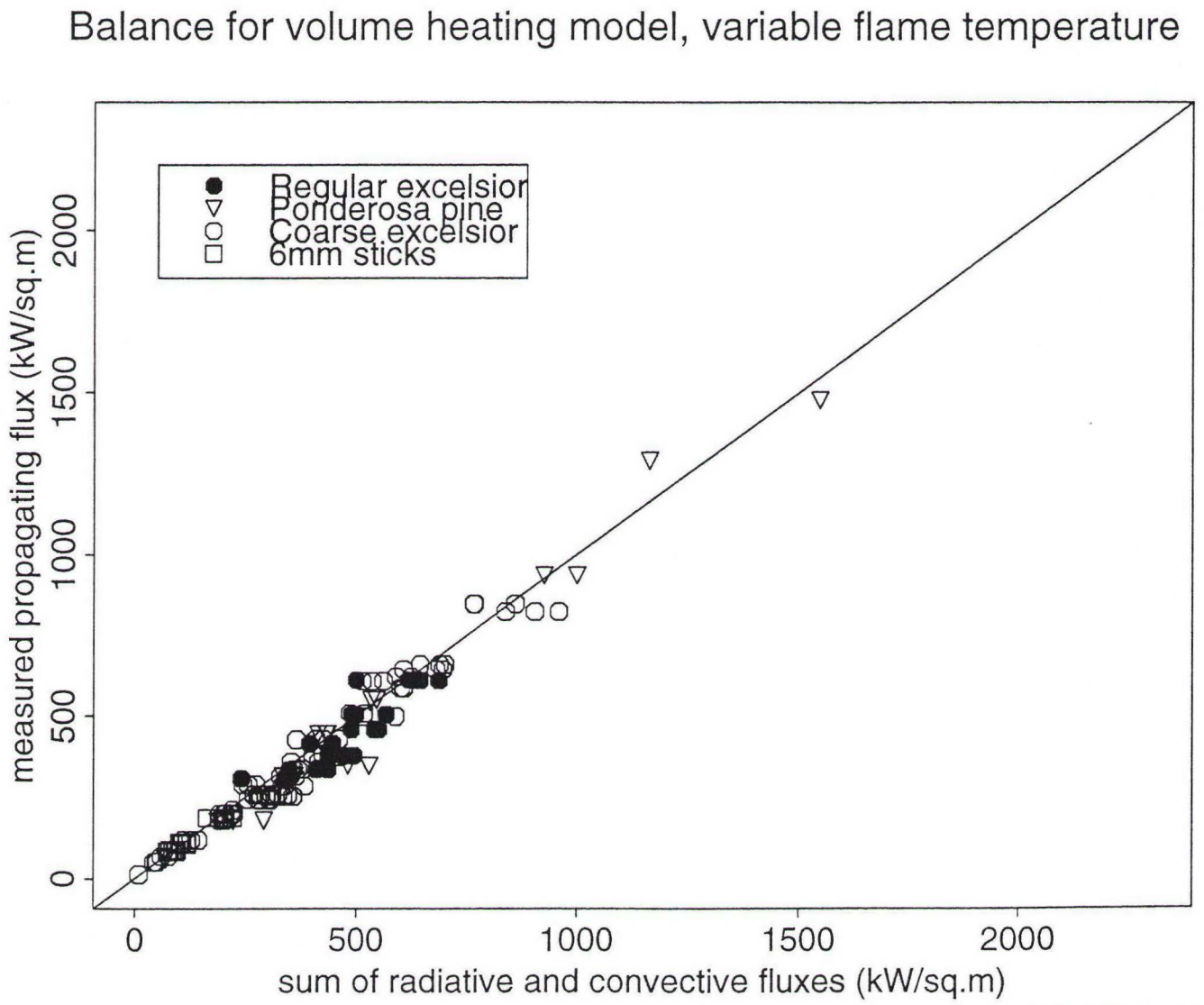

Balance for volume heating model, variable flame temperature
Regular excelsior
Ponderosa pine
Coarse excelsior
6mm sticks
measured propagating flux (kW/sq.m)
0
500
1000
1500
2000
sum of radiative and convective fluxes (kW/sq.m)

FIGURE 1.10

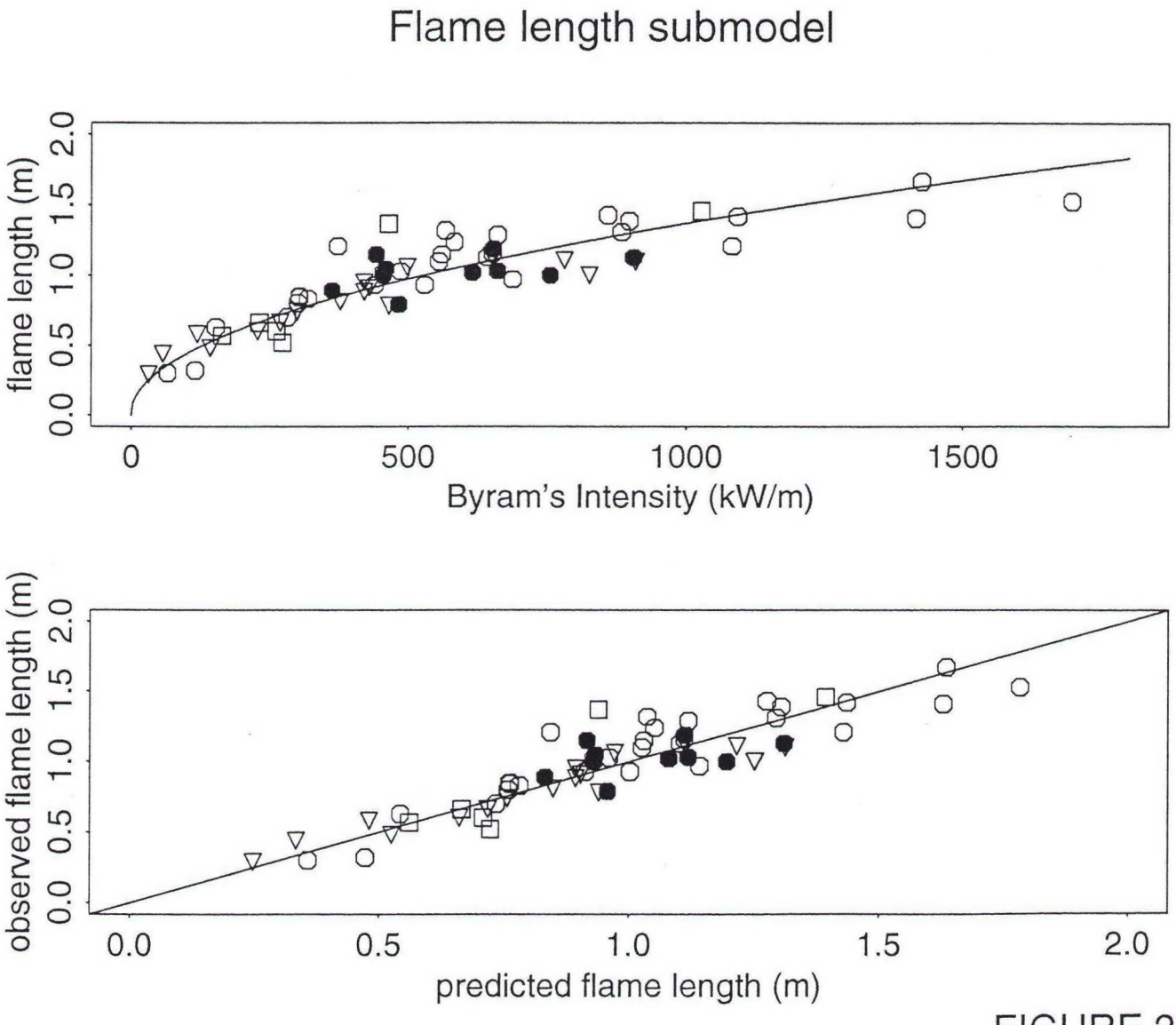

Flame length submodel
flame length (m)
0.0
0.5
1.0
1.5
2.0
0
500
1000
1500
Byram's Intensity (kW/m)
observed flame length (m)
0.0
0.5
1.0
1.5
2.0
0.0
0.5
1.0
1.5
2.0
predicted flame length (m)

FIGURE 2.1

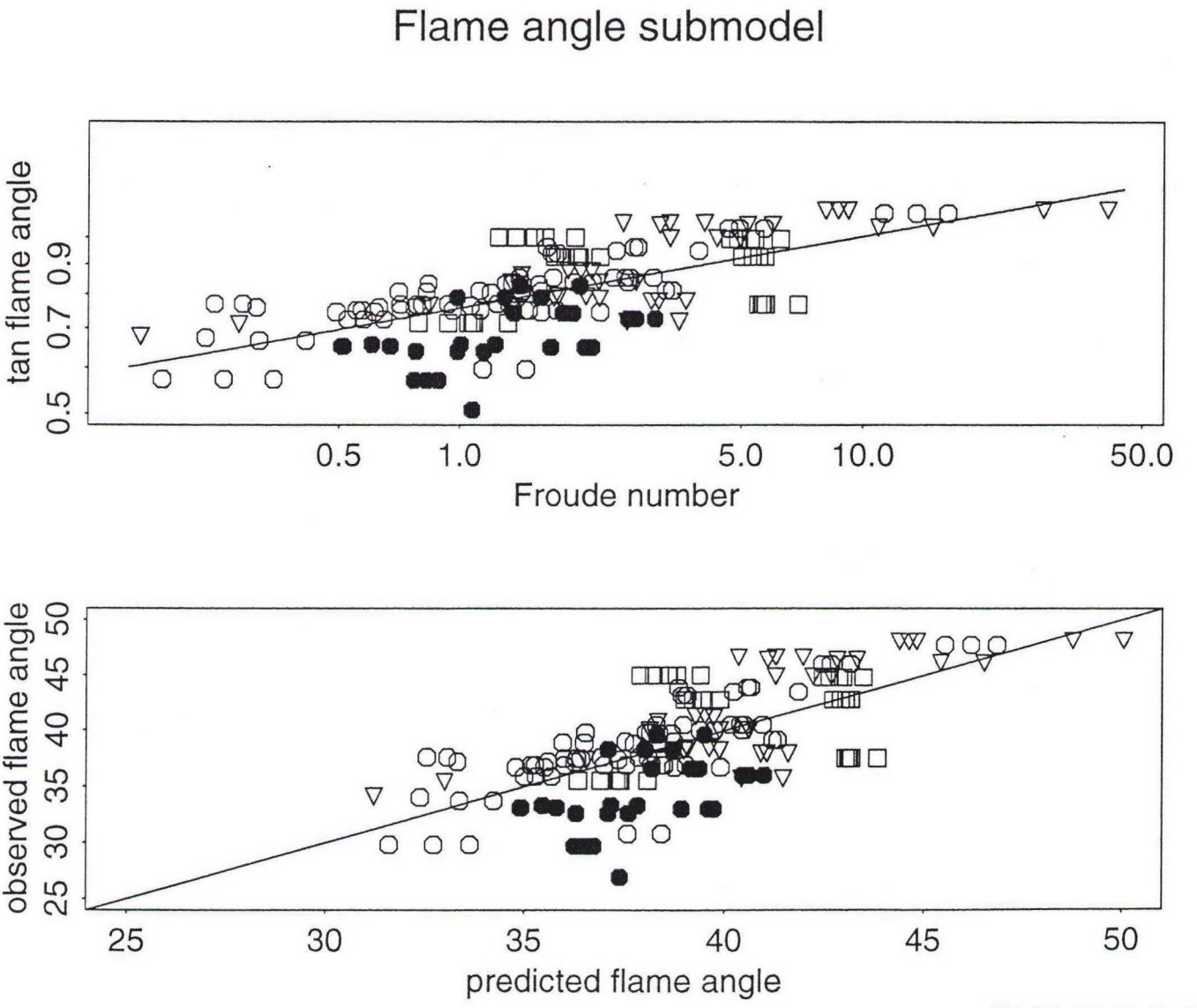

Flame angle submodel
tan flame angle
0.5
0.7
0.9
0.5
1.0
5.0
10.0
50.0
Froude number
observed flame angle
25
30
35
40
45
50
25
30
35
40
45
50
predicted flame angle

FIGURE 2.2

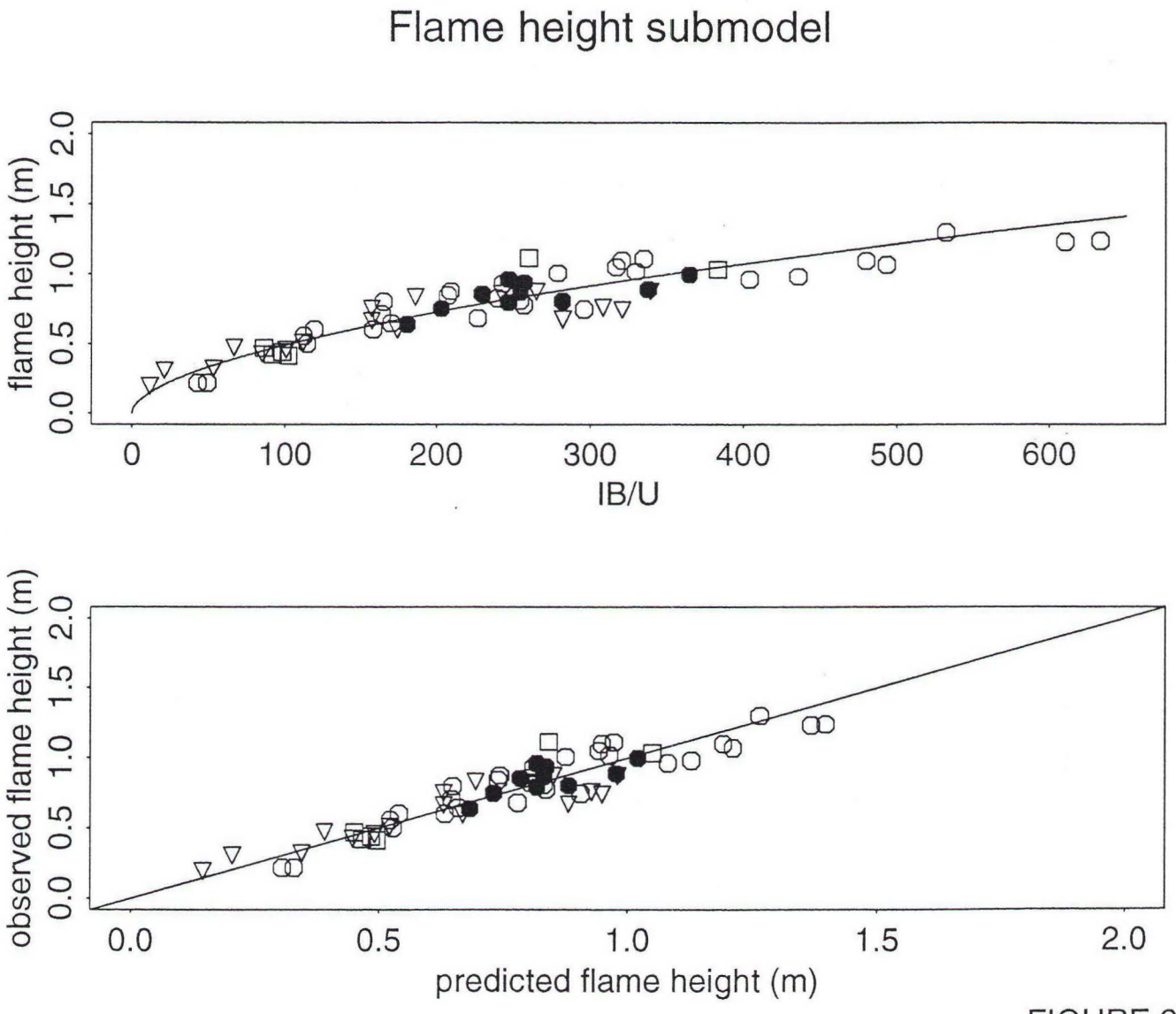

Flame height submodel
flame height (m)
0.0
0.5
1.0
1.5
2.0
0
100
200
300
400
500
600
IB/U
observed flame height (m)
0.0
0.5
1.0
1.5
2.0
predicted flame height (m)

FIGURE 2.3

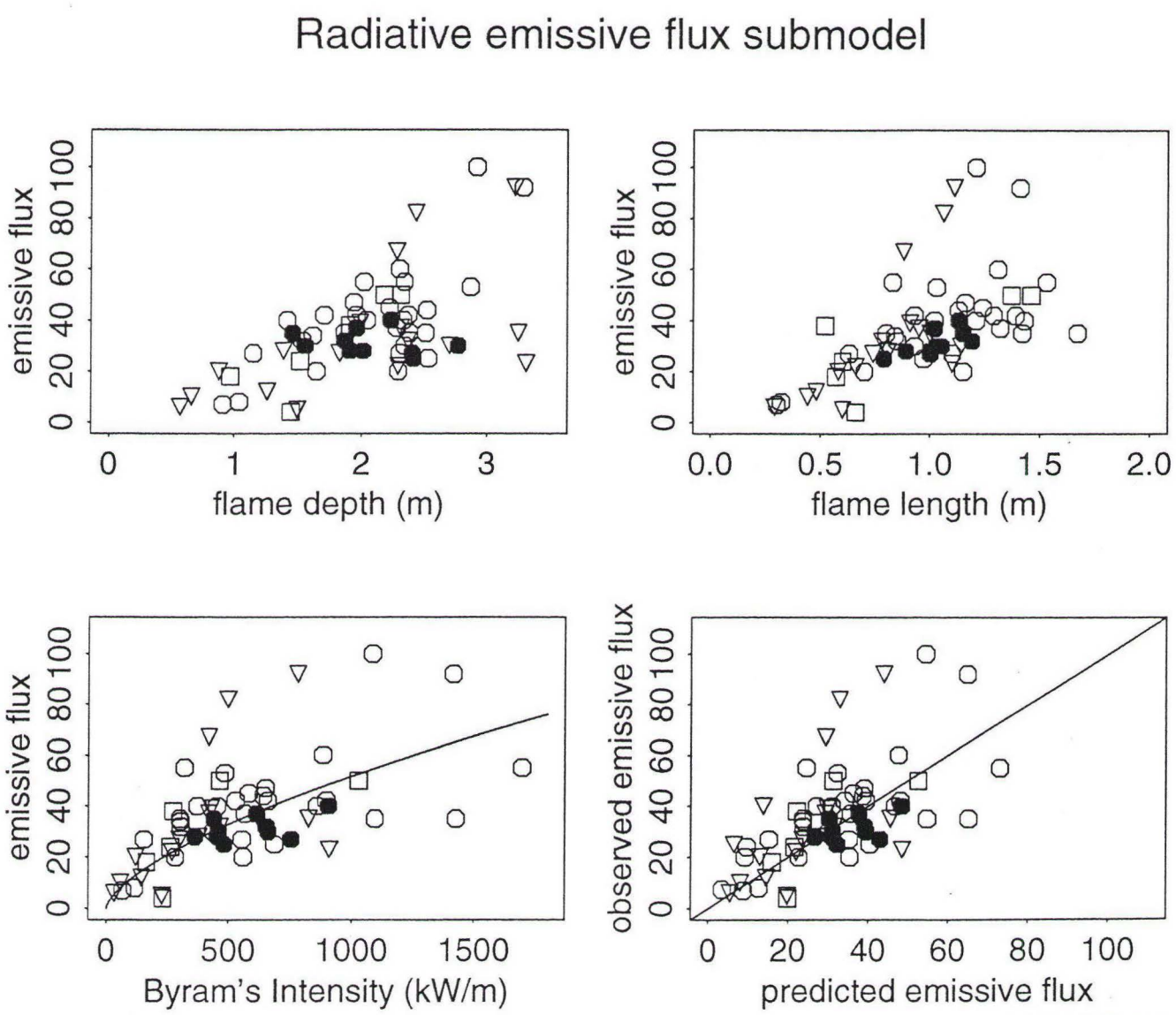

Radiative emissive flux submodel
emissive flux
0 20 40 60 80 100
0 1 2 3
flame depth (m)
emissive flux
0 20 40 60 80 100
0.0 0.5 1.0 1.5 2.0
flame length (m)
emissive flux
0 20 40 60 80 100
0 500 1000 1500
Byram's Intensity (kW/m)
observed emissive flux
0 20 40 60 80 100
0 20 40 60 80 100
predicted emissive flux

FIGURE 2.4

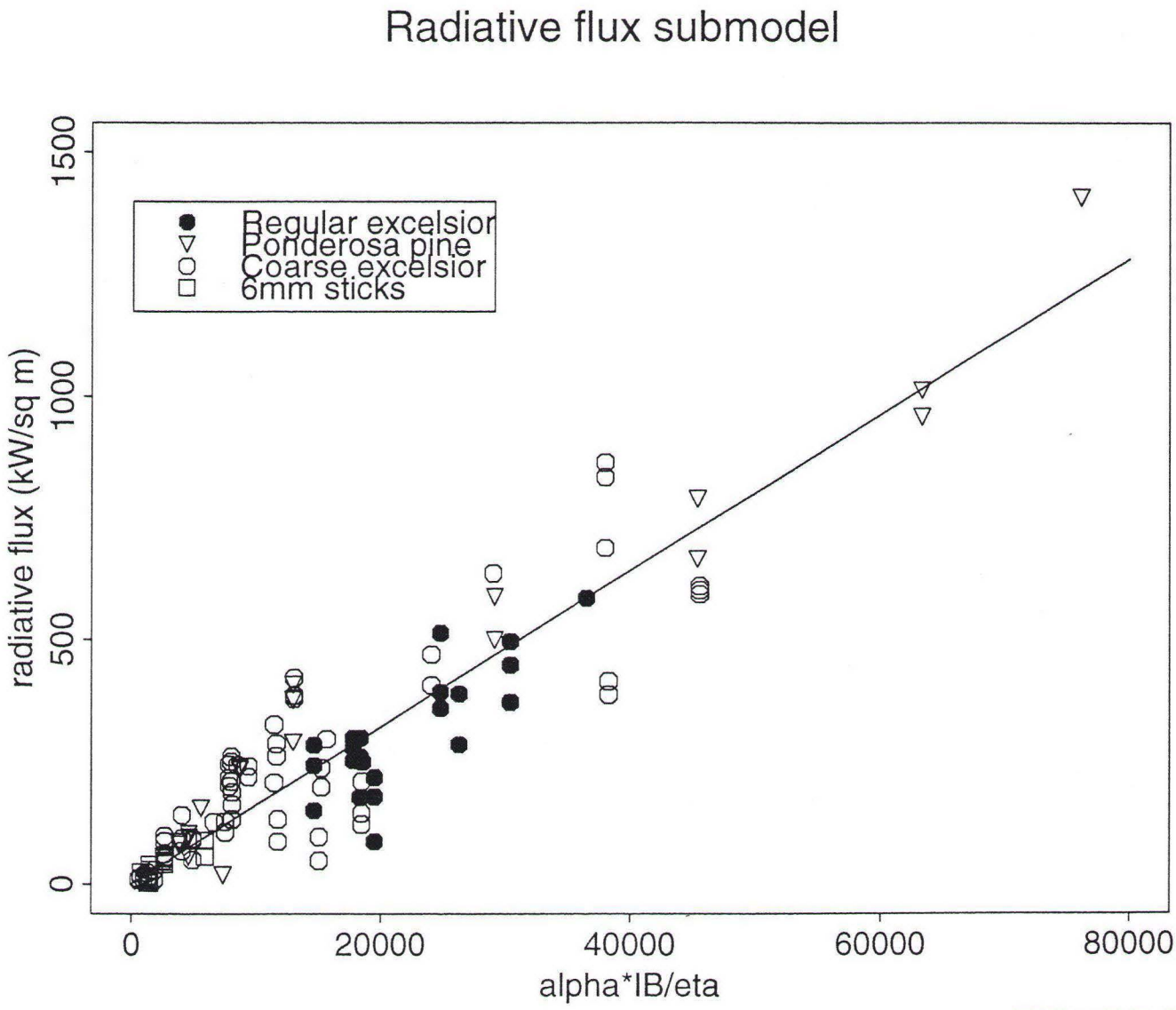

Radiative flux submodel
Regular excelsior
Ponderosa pine
Coarse excelsior
6mm sticks
radiative flux (kW/sq m)
0
500
1000
1500
0
20000
40000
60000
80000
alpha*IB/eta

FIGURE 2.5

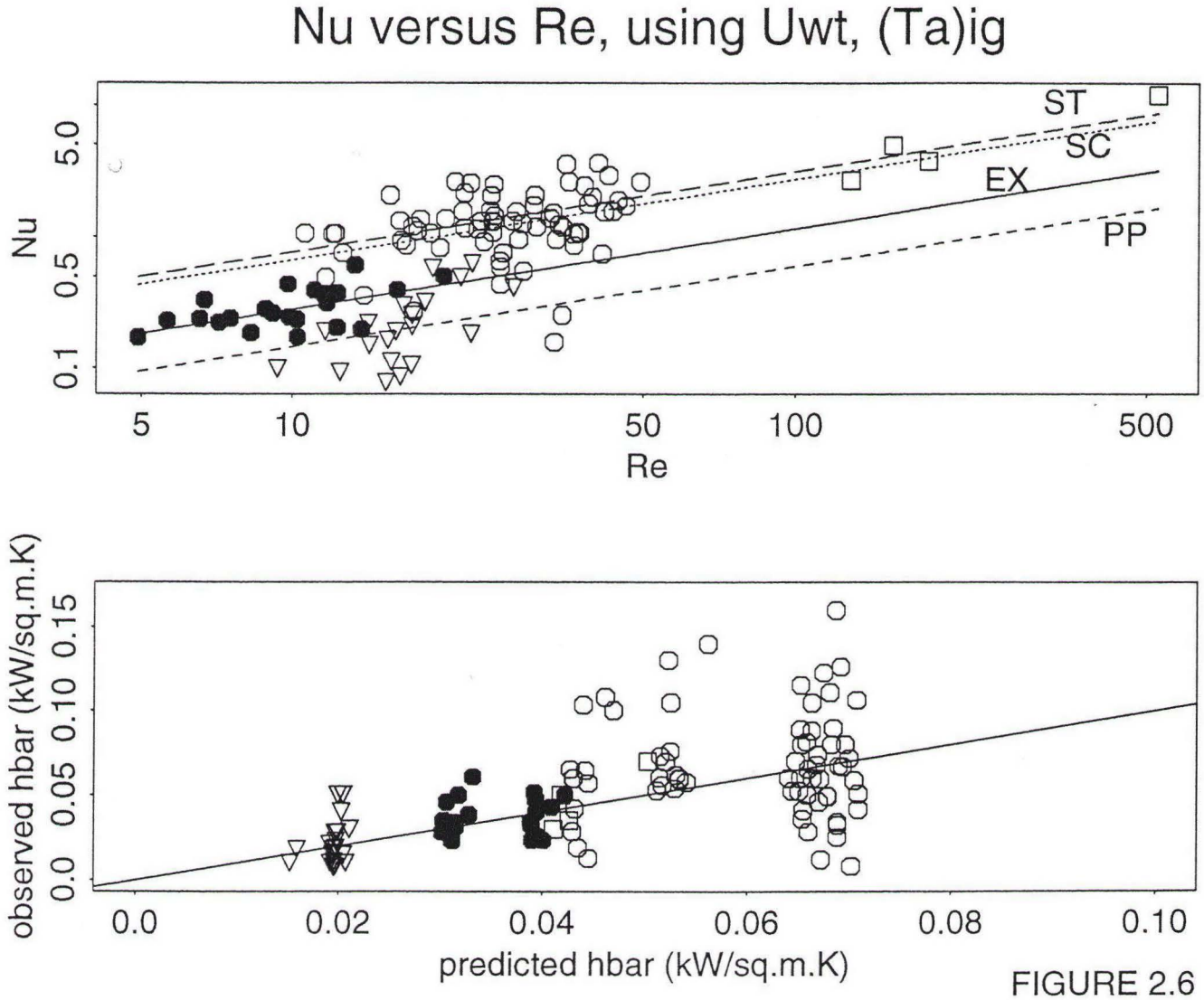

Nu versus Re, using Uwt, (Ta)ig
Nu
0.1
0.5
5.0
ST
SC
EX
PP
5
10
50
100
500
Re
observed hbar (kW/sq.m.K)
0.0
0.05
0.10
0.15
0.0
0.02
0.04
0.06
0.08
0.10
predicted hbar (kW/sq.m.K)

FIGURE 2.6

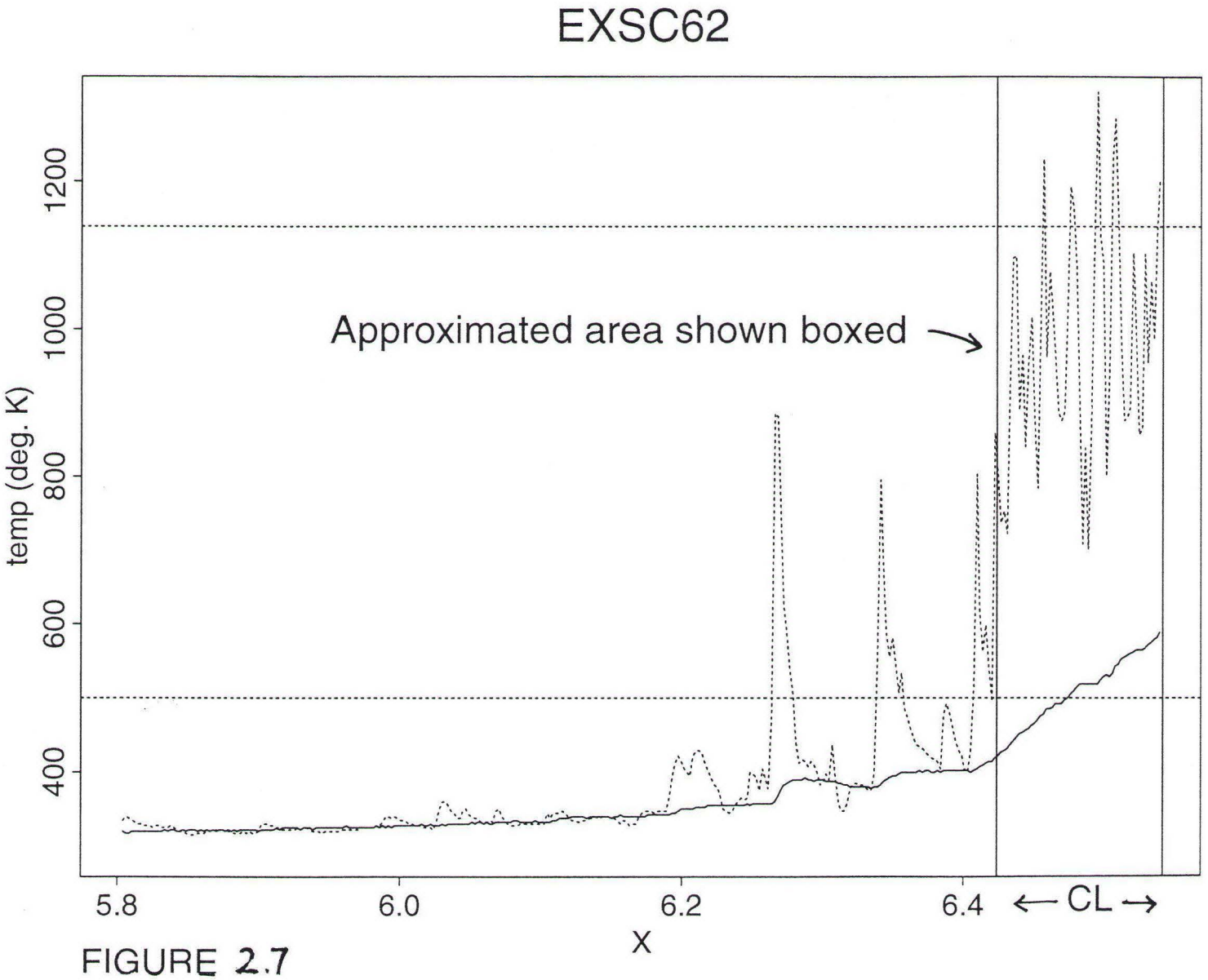

EXSC62
Approximated area shown boxed
temp (deg. K)
400
600
800
1000
1200
5.8
6.0
6.2
6.4
← CL →
X

FIGURE 2.7

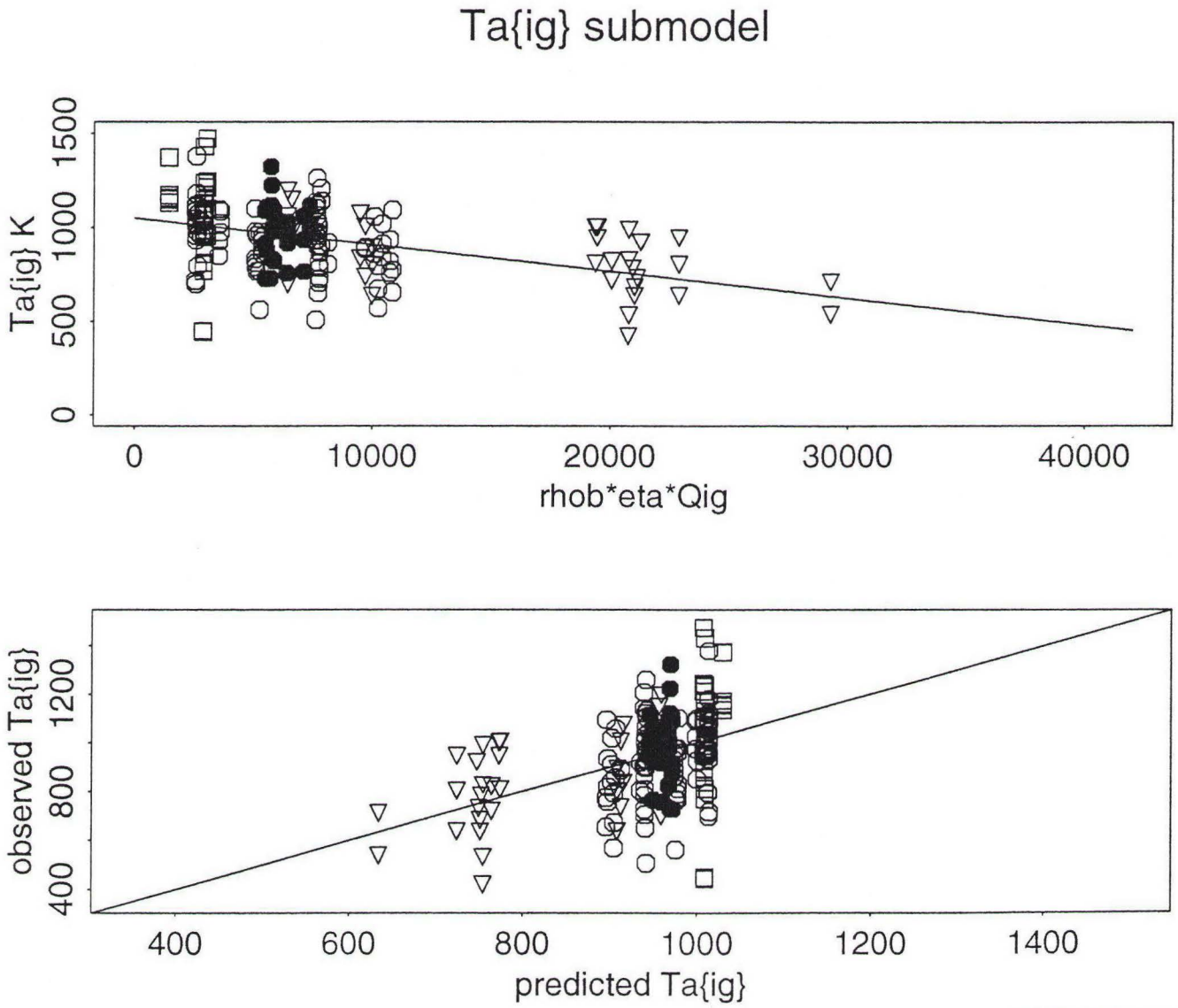

Ta{ig} submodel
Ta{ig} K
0
500
1000
1500
0
10000
20000
30000
40000
rhob*eta*Qig
observed Ta{ig}
400
800
1200
400
600
800
1000
1200
1400
predicted Ta{ig}

FIGURE 2.8

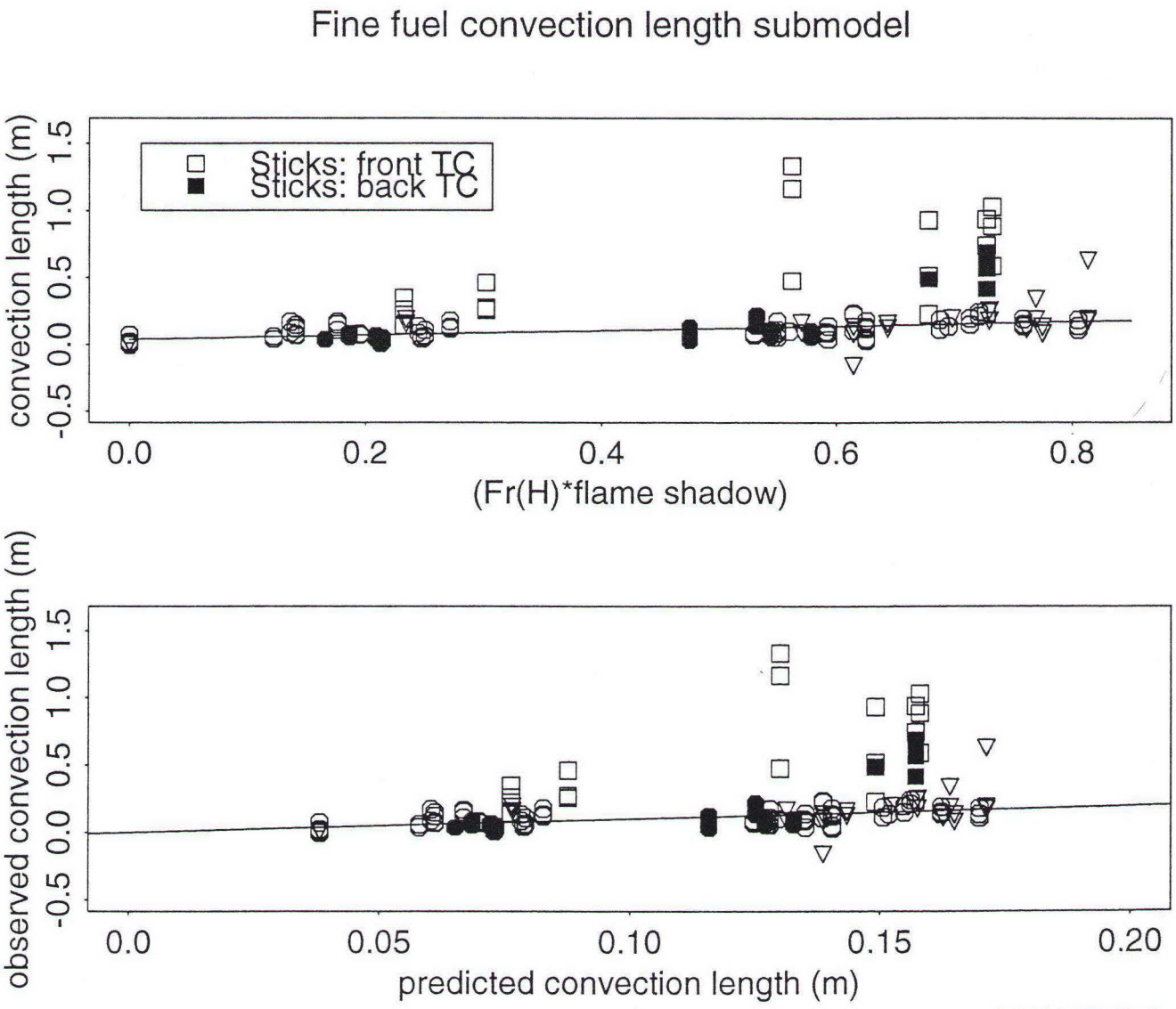

Fine fuel convection length submodel
Sticks: front TC
Sticks: back TC
convection length (m)
-0.5 0.0 0.5 1.0 1.5
0.0 0.2 0.4 0.6 0.8
(Fr(H)*flame shadow)
observed convection length (m)
-0.5 0.0 0.5 1.0 1.5
0.0 0.05 0.10 0.15 0.20
predicted convection length (m)

FIGURE 2.10

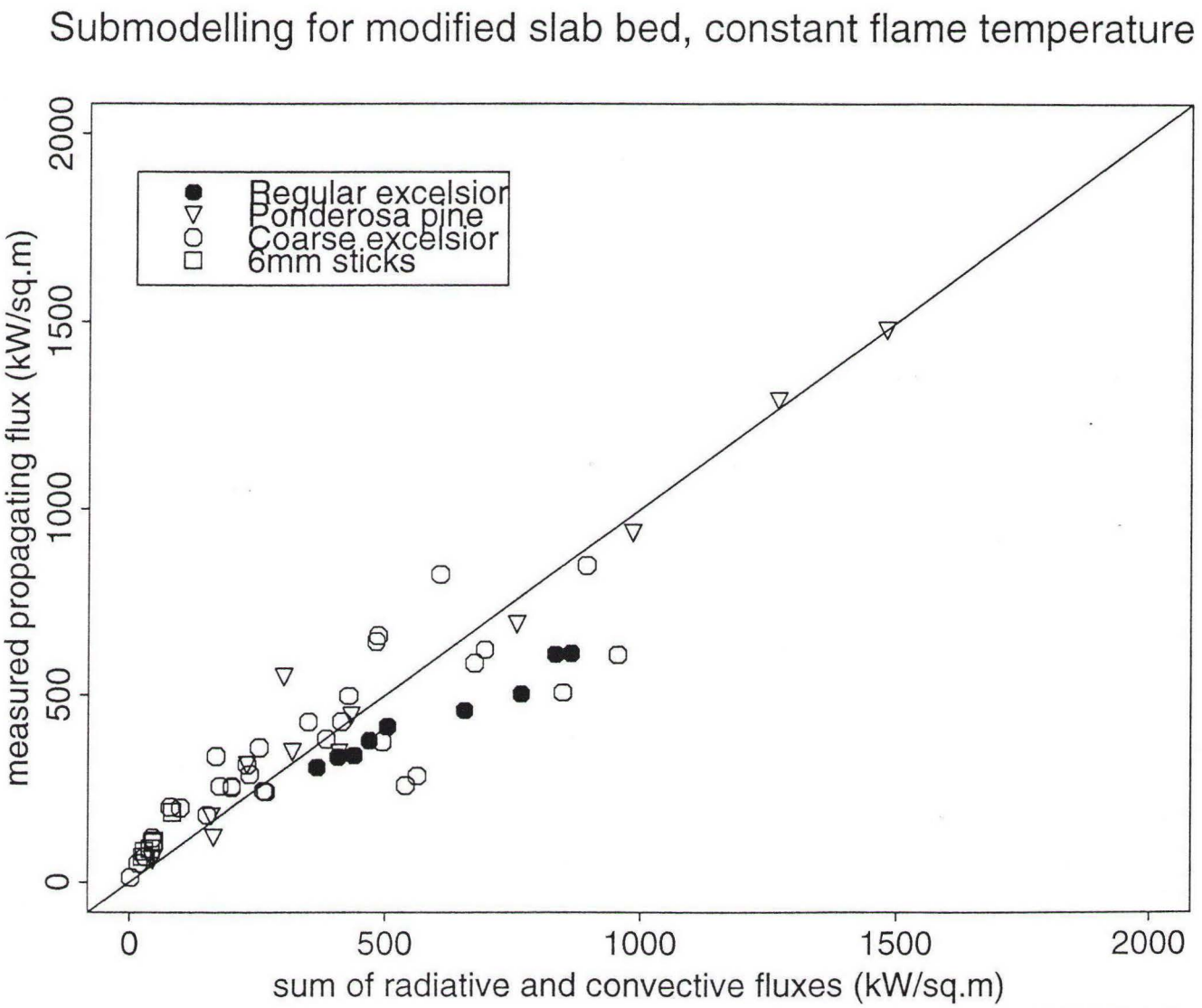

Submodelling for modified slab bed, constant flame temperature
Regular excelsior
Ponderosa pine
Coarse excelsior
6mm sticks
measured propagating flux (kW/sq.m)
sum of radiative and convective fluxes (kW/sq.m)
0
500
1000
1500
2000

FIGURE 2.11

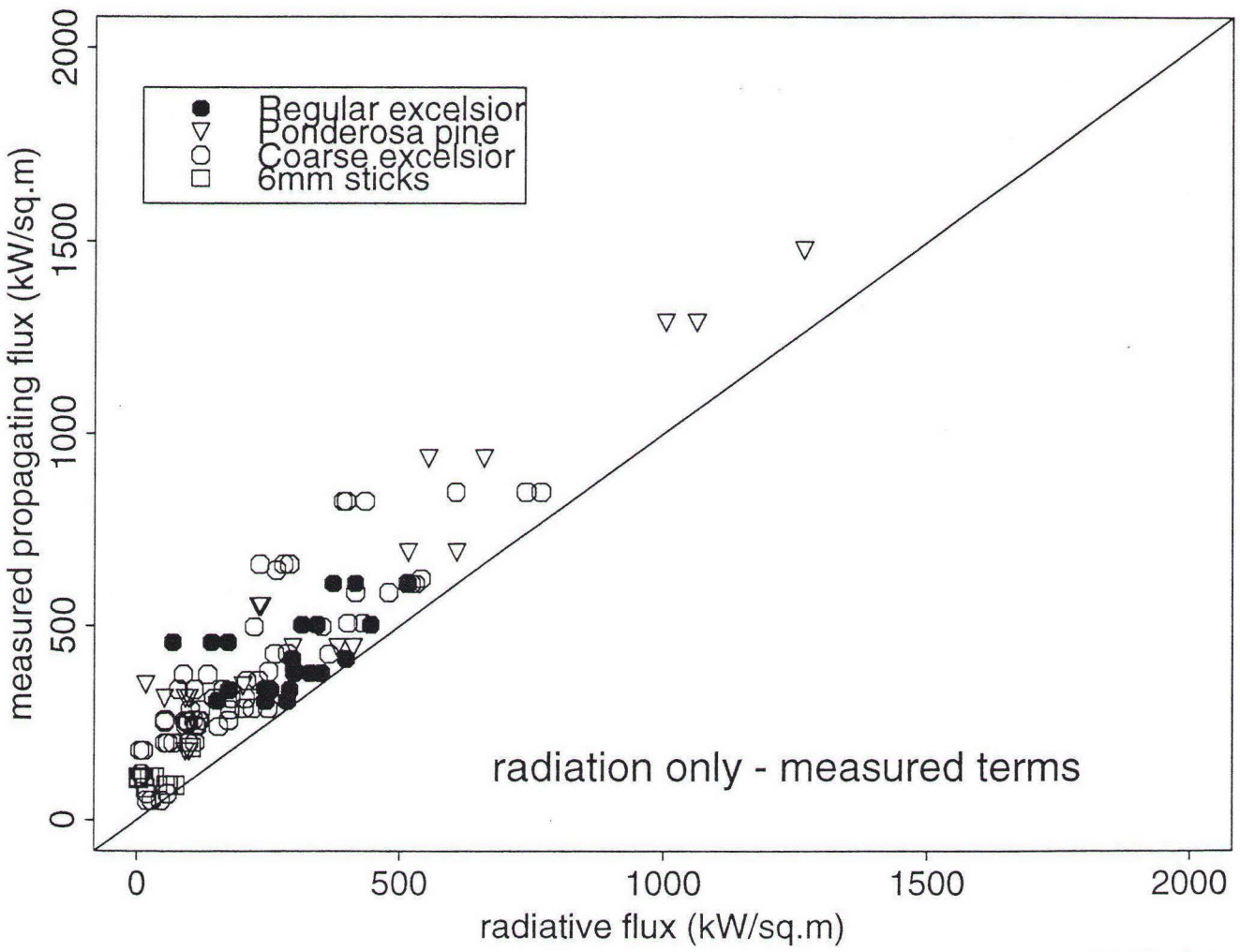

Radiation terms for modified slab bed, constant flame temperature
Regular excelsior
Ponderosa pine
Coarse excelsior
6mm sticks
radiation only - measured terms
measured propagating flux (kW/sq.m)
radiative flux (kW/sq.m)
0
500
1000
1500
2000

FIGURE 2.12

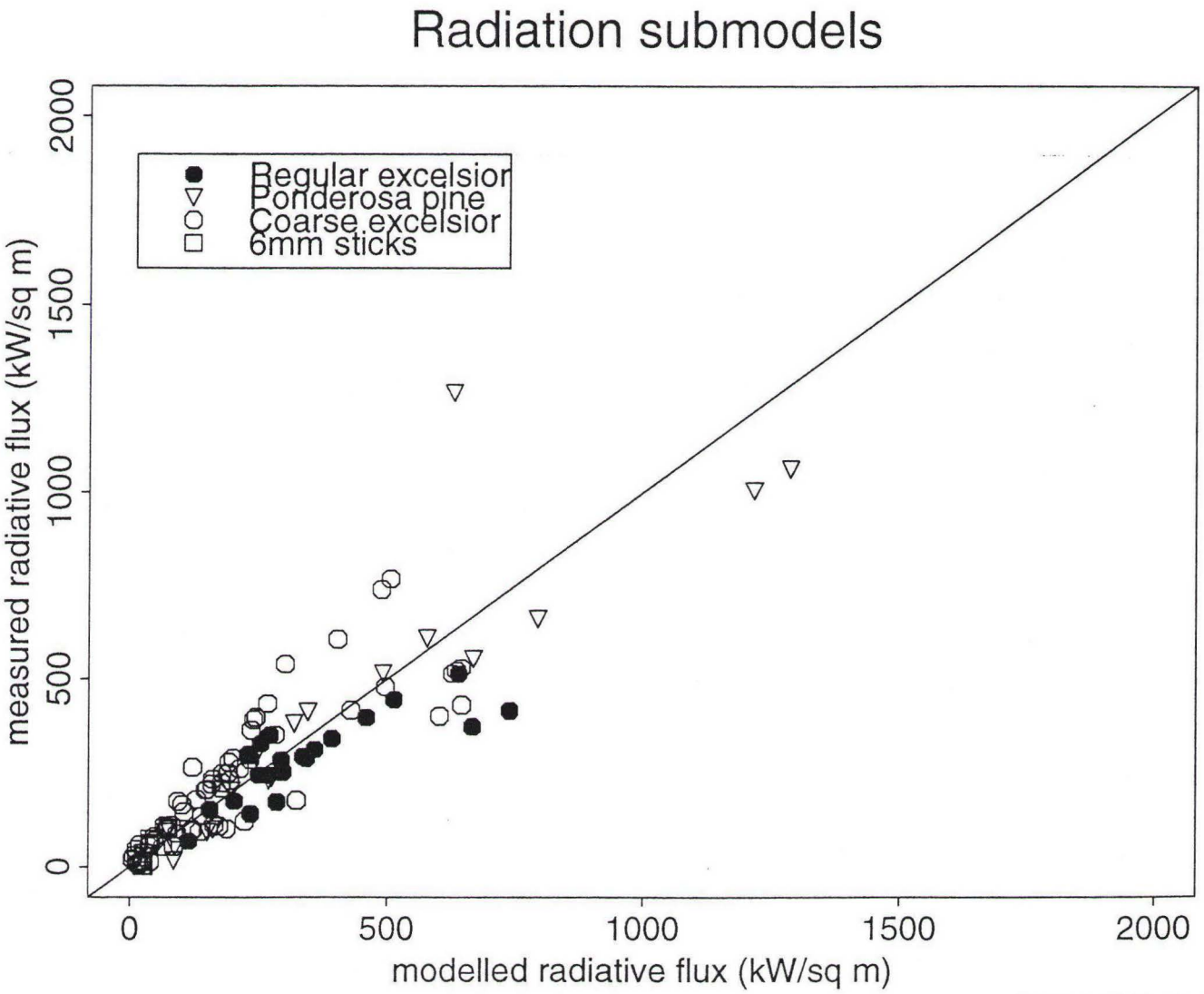

Radiation submodels
Regular excelsior
Ponderosa pine
Coarse excelsior
6mm sticks
measured radiative flux (kW/sq m)
modelled radiative flux (kW/sq m)
0
500
1000
1500
2000

FIGURE 2.13

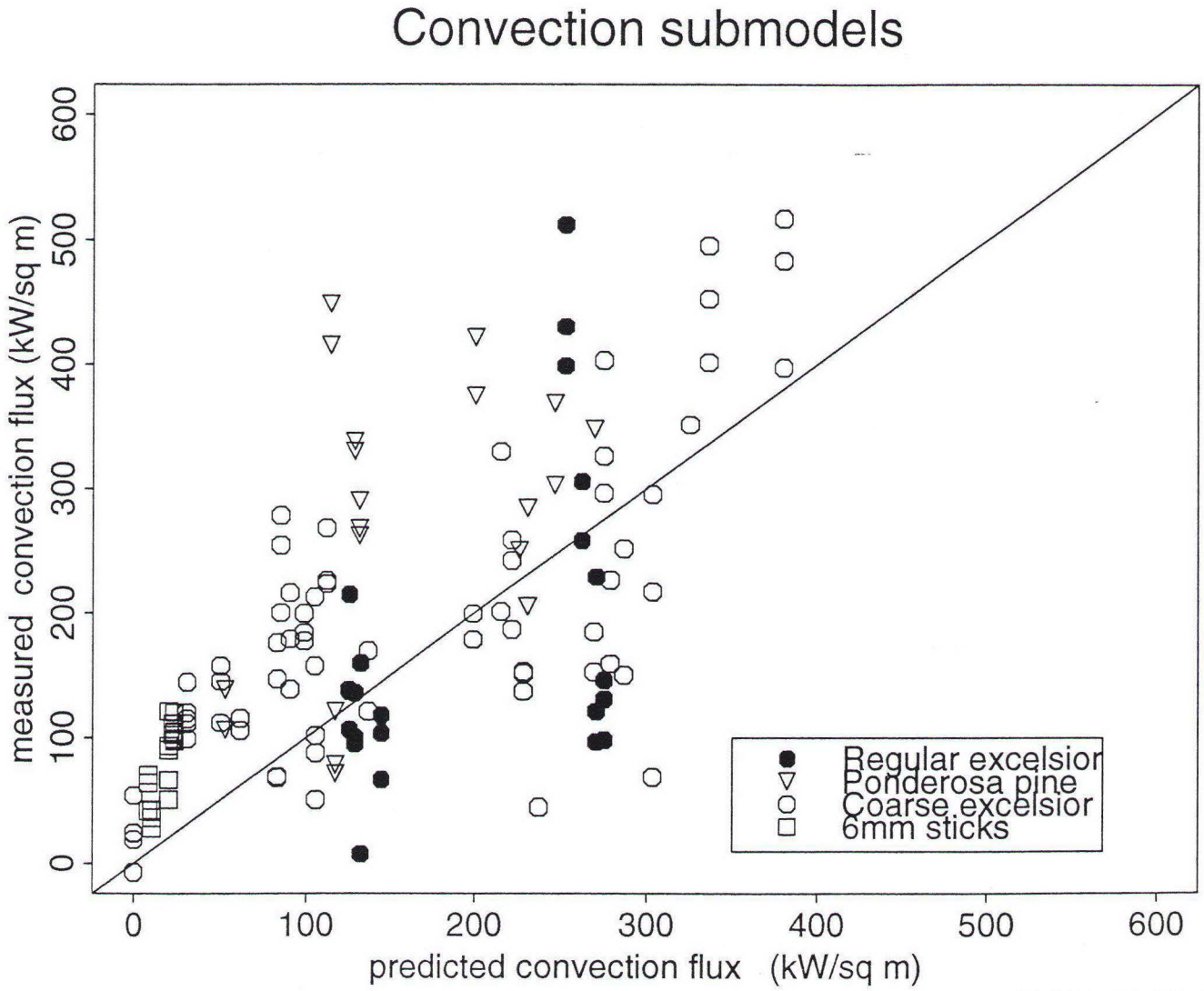

Convection submodels
measured convection flux (kW/sq m)
predicted convection flux (kW/sq m)
0
100
200
300
400
500
600
Regular excelsior
Ponderosa pine
Coarse excelsior
6mm sticks

FIGURE 2.14

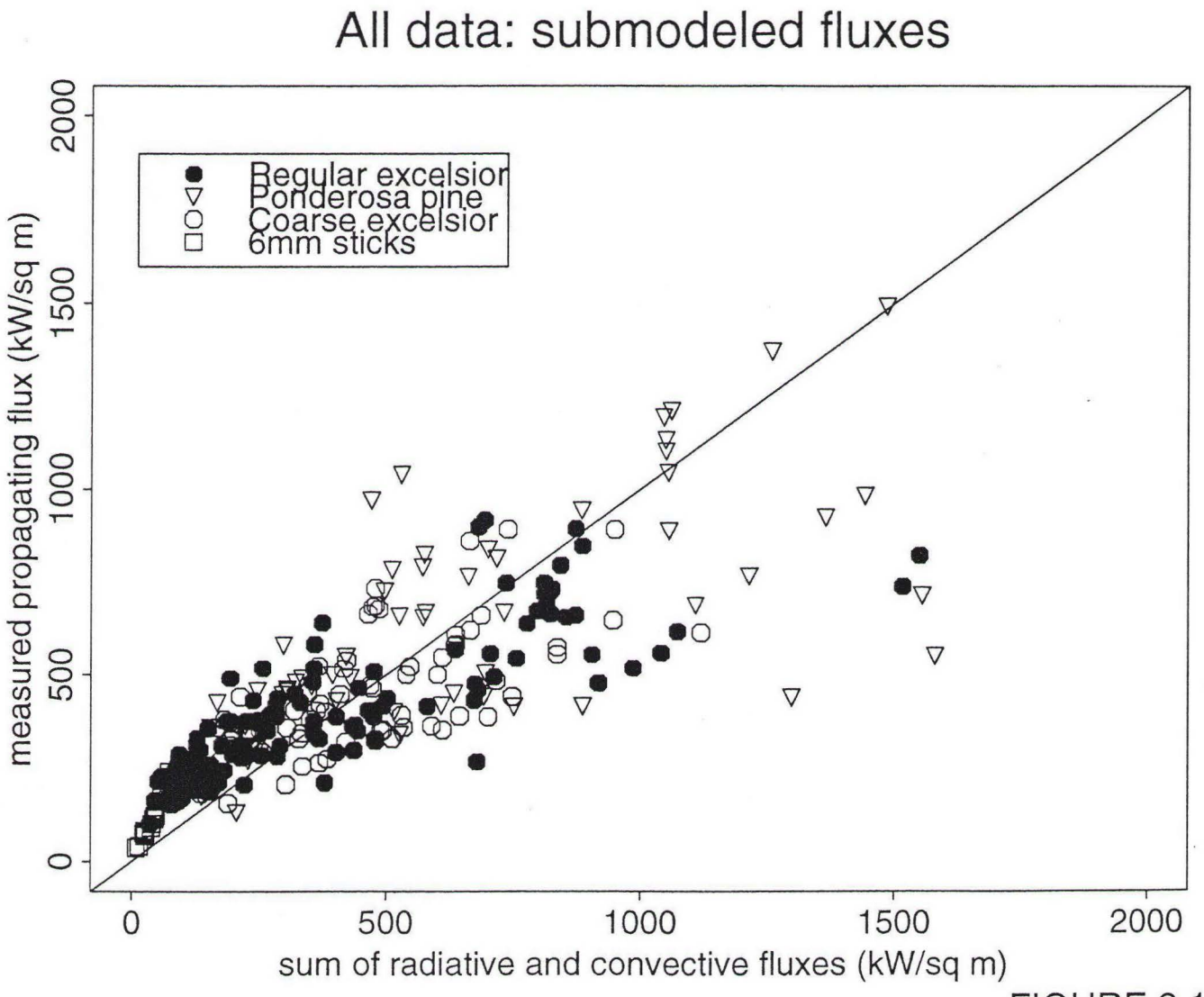

All data: submodeled fluxes
Regular excelsior
Ponderosa pine
Coarse excelsior
6mm sticks
measured propagating flux (kW/sq m)
0
500
1000
1500
2000
sum of radiative and convective fluxes (kW/sq m)

FIGURE 2.15

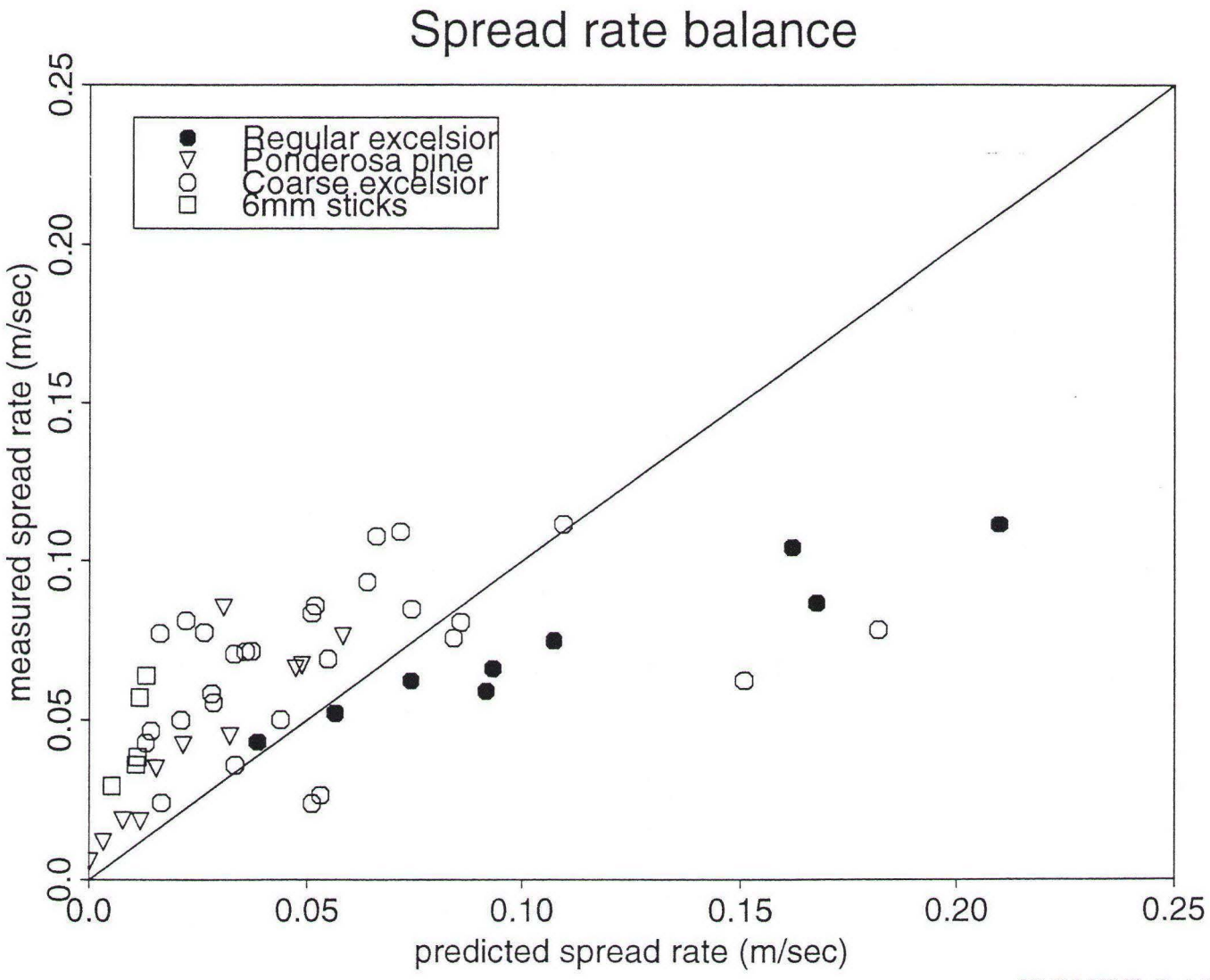

Spread rate balance
Regular excelsior
Ponderosa pine
Coarse excelsior
6mm sticks
measured spread rate (m/sec)
predicted spread rate (m/sec)
0.0
0.05
0.10
0.15
0.20
0.25

FIGURE 2.16

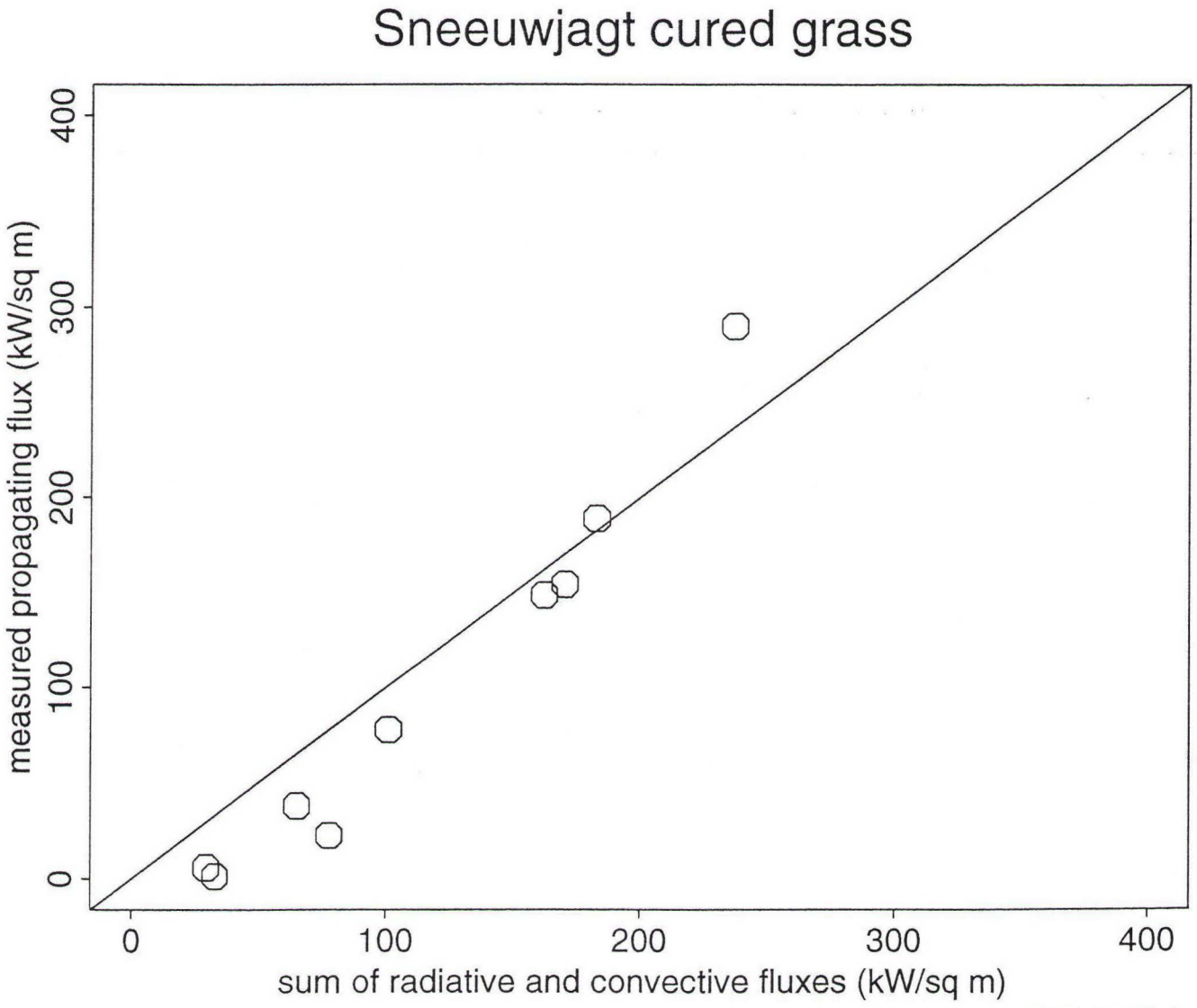

Sneeuwjagt cured grass
measured propagating flux (kW/sq m)
0
100
200
300
400
0
100
200
300
400
sum of radiative and convective fluxes (kW/sq m)

FIGURE 2.17

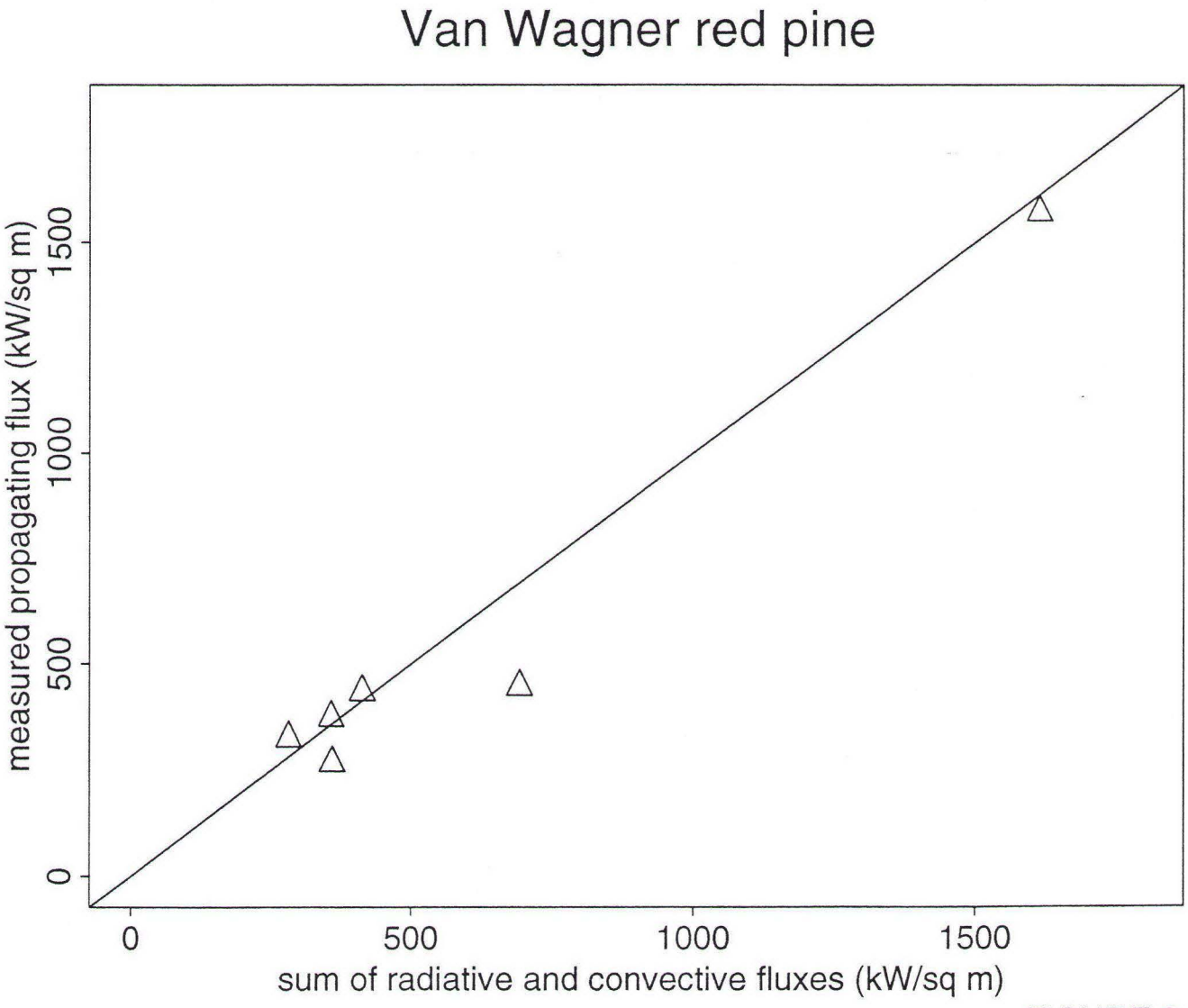

Van Wagner red pine
measured propagating flux (kW/sq m)
0
500
1000
1500
0
500
1000
1500
sum of radiative and convective fluxes (kW/sq m)

FIGURE 2.18

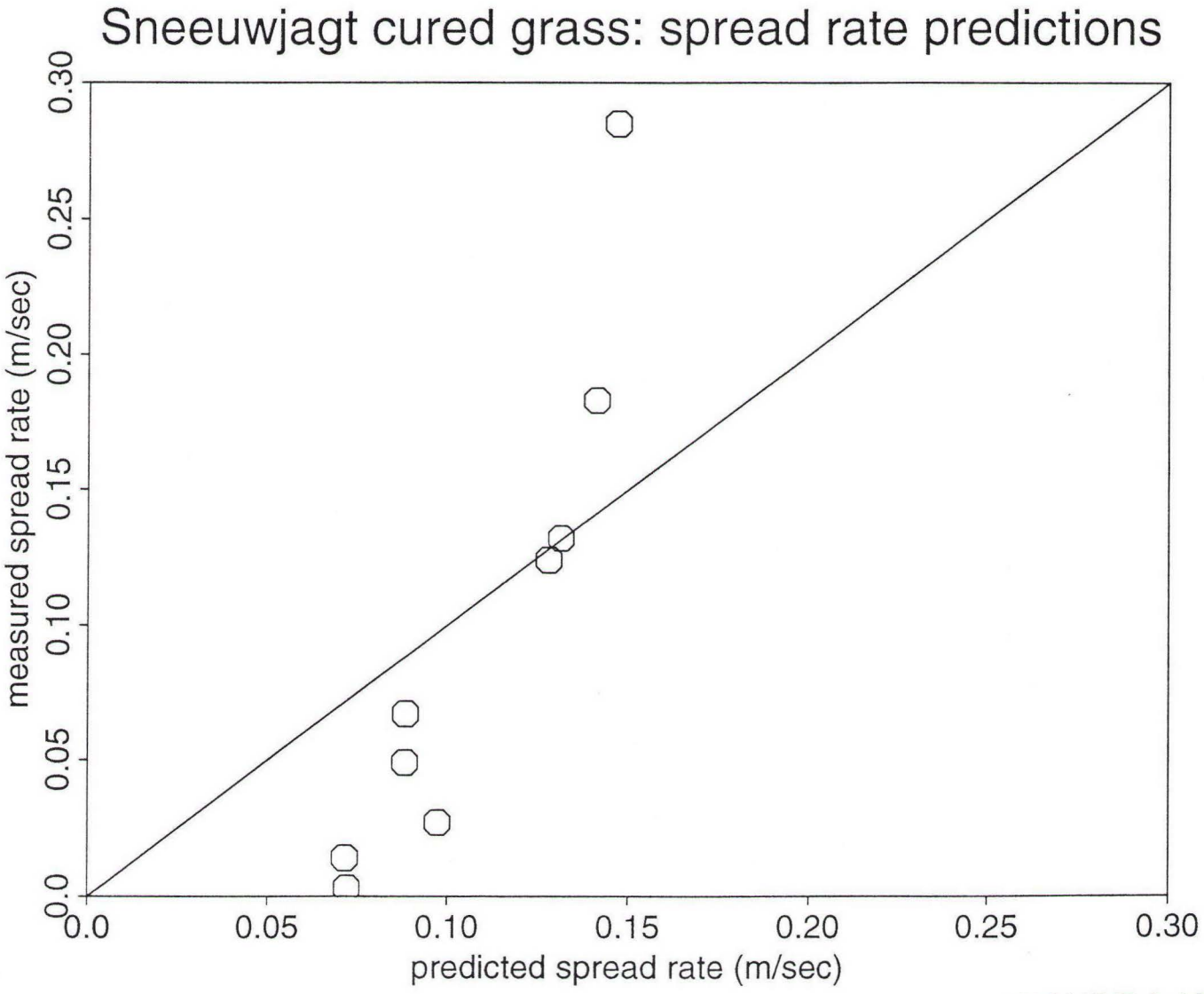

Sneeuwjagt cured grass: spread rate predictions
measured spread rate (m/sec)
0.0
0.05
0.10
0.15
0.20
0.25
0.30
predicted spread rate (m/sec)

FIGURE 2.19

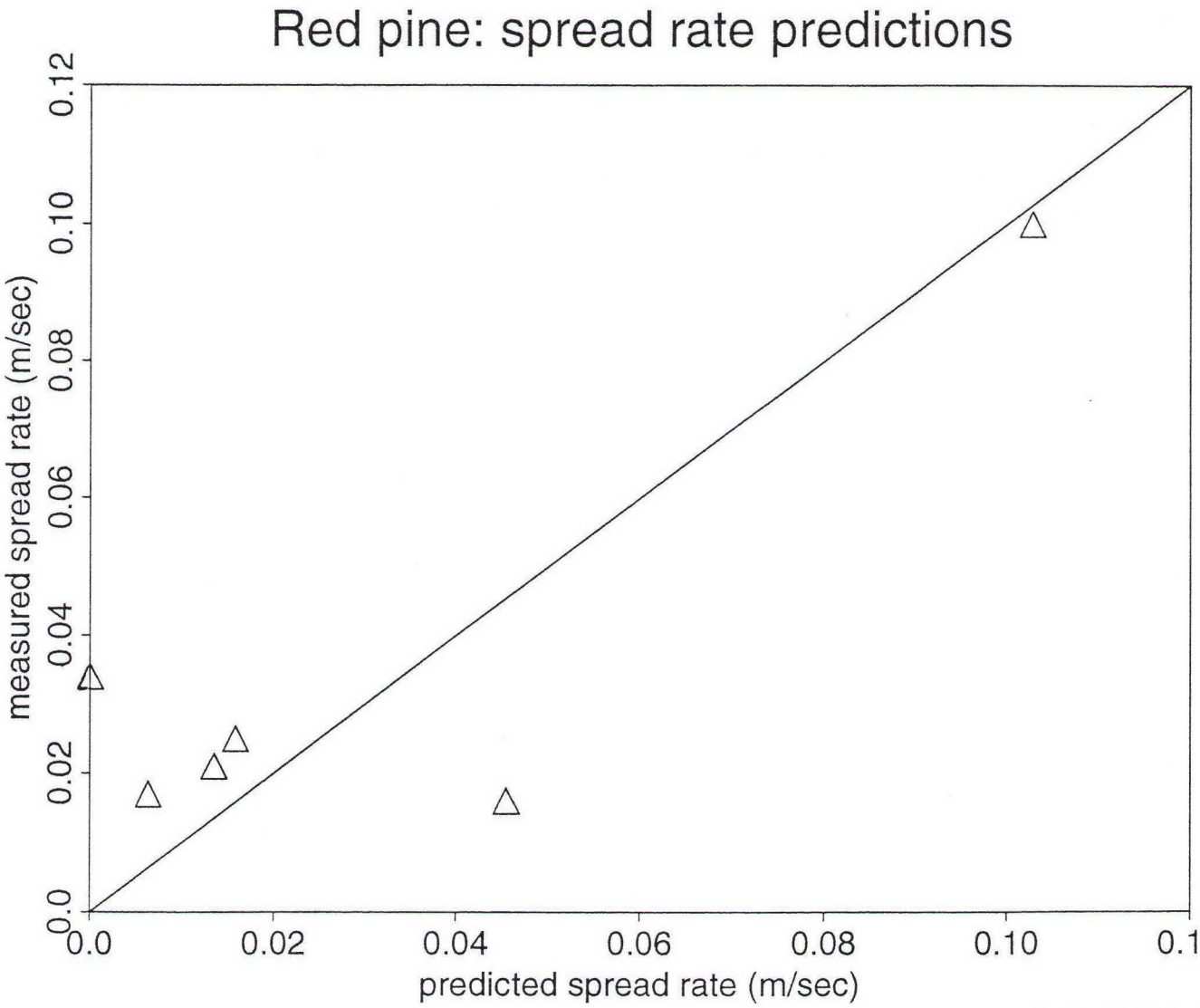

Red pine: spread rate predictions
measured spread rate (m/sec)
predicted spread rate (m/sec)
0.0
0.02
0.04
0.06
0.08
0.10
0.12

FIGURE 2.20

Property of
National FS Library
USDA Forest Service
240 W Prospect Rd
Fort Collins CO 80526